CERTIFIED REDUCED BASIS METHOD FOR THE ELECTRIC FIELD INTEGRAL EQUATION

JAN S. HESTHAVEN *, BENJAMIN STAMM †, AND SHUN ZHANG ‡

Abstract. In [5], a reduced basis method (RBM) for the electric field integral equation (EFIE) based on the boundary element method (BEM) is developed, based on a simplified a posteriori error estimator for the Greedy-based snapshot selection. In this paper, we extend this work and propose a certified RBM for the EFIE based on a mathematically rigorous a posteriori estimator. The main difficulty of the certified method is that the intrinsic solution space of the EFIE is $\boldsymbol{H}_{\mathrm{div}}^{-\frac{1}{2}}(\Gamma)$, with a norm that is not computable in practice. Since the measured error consists of the difference between the reduced basis solution and the boundary element solution, which is a member of the discrete boundary element space, we clarify that the intrinsic norm can be replaced by alternative norms, in this work the $\boldsymbol{H}(\mathrm{div})$-norm, that are computable without degrading the quality of the error estimator. A successive constraint method (SCM) for complex matrices is discussed in detail and numerical tests for the SCM and certified RBM are performed to confirm the analysis.

1. Introduction. Many applications related to computational optimization, control, and design require the ability to rapidly, and accurately solve parameterized problems many times for different parameter values within a given parametric domain. The reduced basis method (RBM) [11, 13] is a very accurate and efficient method for such scenarios allowing a mathematically rigorous error control of the applied model reduction.

In [5], a reduced basis method (RBM) for parameterized scattering problems in computational electromagnetics for the electric field integral equation (EFIE) [2, 6, 7], discretized using the boundary element method, is proposed. As is standard for RBMs a greedy algorithm, based on an a posteriori estimator, is employed to assemble the low dimensional (reduced basis) approximation space. The quality of these estimates has a direct impact on the approximation properties of the reduced basis. In [5], a simple L^2-norm of the residual is used as an error estimator, neglecting the parameter dependence of the involved inf-sup stability constant of the BEM. For the EFIE with the wave number being a parameter, this constant can be arbitrarily close to zero for some configurations and a uniform lower bound may thus lead to very conservative error estimates. Thus, to improve the quality of the error estimator and recover a practical certified RBM, we have to design the error estimator carefully to incorporate the stability constant.

In [4, 9, 11, 13], the general background for a posteriori error estimators for the reduced basis method is presented. In these papers, the intrinsic norm of the solution space is used to measure the error. For example, the H^1-norm is used for diffusion equations [11] and the $\boldsymbol{H}(\mathrm{curl})$-norm is used for Maxwell's equations [4]. For most problems, this intrinsic norm is the natural choice as we often have some a priori stability estimates based on these intrinsic norms. In general, the coercivity or the inf-sup stability constant has advantageous properties, making the computation of the coercivity or the inf-sup stability constant in these intrinsic norms more stable.

*Division of Applied Mathematics, Box F, Brown University, 182 George St., Providence, RI 02912, Jan.Hesthaven@Brown.edu. This work is supported in part by OSD/AFOSR FA9550-09-1-0613.

†Department of Mathematics, University of California, Berkeley, Berkeley, CA 94720, stamm@math.berkeley.edu.

‡Division of Applied Mathematics, Box F, Brown University, 182 George St., Providence, RI 02912, Shun_Zhang@Brown.edu.

For the EFIE, the intrinsic solution space is $\boldsymbol{H}_{\mathrm{div}}^{-\frac{1}{2}}(\Gamma)$ [2, 7], a dual space on the surface Γ. The corresponding norm is defined as a dual norm. The computation of dual norms is very difficult in practice if not computationally prohibitive, see [10] for a computation of the $H^{-1/2}$-norm based on multilevel refinements. In addition, the a priori estimation of the EFIE is very weak and the existence and uniqueness of the solution are based on the Fredholm alternative theory. There is no a priori estimation for the inf-sup constants for the EFIE and thus the benefit of using the intrinsic norm is less clear.

However, we may use other suitable norms. For a particular parameter value, the model reduction error is measured as the difference between the reduced basis solution and the discrete boundary element solution. Both solutions are discrete and can be measured by some simpler and computable norm. In our case, the discrete boundary element space is the lowest order complex Raviart-Thomas space, which is a conforming subspace of $\boldsymbol{H}_{\mathrm{div}}^{0}(\Gamma)$ equipped with an easily computable $\boldsymbol{H}(\mathrm{div})$-norm. In what follows, we adopt this norm to measure the model reduction error and we shall demonstrate that this does not adversely impact the accuracy of the error estimator.

The corresponding inf-sup stability constants with respect to the $\boldsymbol{H}(\mathrm{div})$-norm are computed by the successive constraint method (SCM) [3, 4, 8]. Different from the presentation in [3], where the real and imaginary parts of a complex matrix are decoupled in the SCM, we improve the algorithm by fully utilizing the properties of Hermitian matrices.

What remains of this paper is organized as follows. In Section 2 we briefly outline the electric field integral equation (EFIE), the boundary element methods (BEM), and the reduced basis method (RBM) for the EFIE. We develop a certified RBM in Section 3, where the error estimator and successive constraint method (SCM) for the complex case is presented in detail. Numerical tests are performed in Section 4 to test the SCM and the certified RBM and Section 5 concludes with a few remarks.

2. EFIE and Reduced Basis Method. In this section, we review the electric field integral equations (EFIE) and the reduced basis methods (RBM). A detailed presentation can be found in [5].

2.1. Governing equations. We consider a configuration in the three-dimensional space, consisting of an obstacle D. The surface of D is denoted by Γ and for each point $\boldsymbol{x} \in \Gamma$ we assign a unitary normal vector $\boldsymbol{n}(\boldsymbol{x})$. If Γ is a closed surface, we chose the exterior normal.

The obstacle D is situated in a homogeneous medium with vanishing conductivity, the free space permittivity $\epsilon_0 = 10^7/(4\pi c^2)\mathrm{F/m}$ and permeability $\mu_0 = 4\pi \times 10^{-7}\mathrm{H/m}$, where $c = 299,792,458$ m/s is the speed of light.

We seek to model the scattering by D of an incident time-harmonic electromagnetic plane wave

$$\boldsymbol{E}^{\mathrm{inc}}(\boldsymbol{x}; k, \hat{\boldsymbol{d}}, \hat{\boldsymbol{p}}) = ik\hat{\boldsymbol{p}}e^{ik\boldsymbol{x}\cdot\hat{\boldsymbol{d}}},$$
$$\boldsymbol{H}^{\mathrm{inc}}(\boldsymbol{x}; k, \hat{\boldsymbol{d}}, \hat{\boldsymbol{p}}) = ik\big(\hat{\boldsymbol{d}}\times\hat{\boldsymbol{p}}\big)e^{ik\boldsymbol{x}\cdot\hat{\boldsymbol{d}}},$$

with $\hat{\boldsymbol{d}} \perp \hat{\boldsymbol{p}}$ and parameterized by the wave-number $k \in \mathbb{R}^+$, direction $\hat{\boldsymbol{d}} \in \mathbb{S}^2$ and polarization $\hat{\boldsymbol{p}} \in \mathbb{R}^3$ where $\mathbb{S}^2$ denotes the unit sphere. We identify any vector perpendicular to $\hat{\boldsymbol{d}}$ to a vector in $\mathbb{R}^2$ by expressing it in a basis that is perpendicular to $\hat{\boldsymbol{d}}$ and denote the set of parameters by $\boldsymbol{\mu} = (k, \hat{\boldsymbol{d}}, \hat{\boldsymbol{p}}) \in \boldsymbol{\mathcal{P}}$ for some fixed parameter domain $\boldsymbol{\mathcal{P}} \subset \mathbb{R}^+ \times \mathbb{S}^2 \times \mathbb{R}^2$. The wavelength of the incident electric and magnetic fields is given by $\lambda = 2\pi/k$.

The total field components $[\boldsymbol{E}, \boldsymbol{H}]$, i.e, the incident and the scattered fields with the latter denoted by $[\boldsymbol{E}^{\text{sca}}, \boldsymbol{H}^{\text{sca}}]$, satisfy the time-harmonic Maxwell equations:

$$\textbf{curl}\, \boldsymbol{E}(\boldsymbol{x}) - i\omega\mu_0 \boldsymbol{H}(\boldsymbol{x}) = \boldsymbol{0}, \qquad \textbf{curl}\, \boldsymbol{H}(\boldsymbol{x}) + i\omega\epsilon_0 \boldsymbol{E}(\boldsymbol{x}) = \boldsymbol{0}, \qquad \boldsymbol{x} \in \mathbb{R}^3 \setminus \overline{D}, \tag{2.1}$$

and the Silver-Müller radiation condition

$$\lim_{|\boldsymbol{x}|\to\infty} [\boldsymbol{H}(\boldsymbol{x})\times\boldsymbol{x} - |\boldsymbol{x}|\boldsymbol{E}(\boldsymbol{x})] = \boldsymbol{0}. \tag{2.2}$$

We assume that the obstacle D is perfectly conducting and hence the tangential component of the total electric field $\boldsymbol{E}$ vanishes on the surface of D, yielding the boundary condition:

$$\boldsymbol{n}(\boldsymbol{x})\times\boldsymbol{E}(\boldsymbol{x}) = -\boldsymbol{n}(\boldsymbol{x})\times\boldsymbol{E}^{\text{inc}}(\boldsymbol{x}), \qquad \boldsymbol{x} \in \Gamma. \tag{2.3}$$

Using the Stratton-Chu representation formula, the scattered electric and the magnetic field can be represented by

$$\begin{aligned}
\boldsymbol{E}^{\text{sca}}(\boldsymbol{x}) &= ikZ \int_\Gamma \left[\mathcal{G}(r;k)\boldsymbol{u}(\boldsymbol{y}) + \tfrac{1}{k^2}\textbf{grad}_{\boldsymbol{x}}\mathcal{G}(r;k)\text{div}_{\Gamma,y}\boldsymbol{u}(\boldsymbol{y})\right] d\boldsymbol{y},\\
\boldsymbol{H}^{\text{sca}}(\boldsymbol{x}) &= -\tfrac{i}{k}\textbf{curl}\, \boldsymbol{E}^{\text{sca}}(\boldsymbol{x}),
\end{aligned}$$

where $\mathcal{G}$ is the fundamental solution of the Helmholtz operator defined by

$$\mathcal{G}(r,k) = \frac{e^{ikr}}{4\pi r}, \quad r = |\boldsymbol{x} - \boldsymbol{y}|.$$

Invoking the boundary condition for $\boldsymbol{E}$ yields the Electric Field Integral Equation (EFIE):

$$\mathbf{T}[\boldsymbol{u}(\boldsymbol{x};\boldsymbol{\mu});\boldsymbol{\mu}] = \mathbf{f}[\boldsymbol{x};\boldsymbol{\mu}], \tag{2.4}$$

where

$$\begin{aligned}
\mathbf{T}[\boldsymbol{u}(\boldsymbol{x};\boldsymbol{\mu});\boldsymbol{\mu}] &= ikZ\,\gamma_t\left(\int_\Gamma \left[\mathcal{G}(r;k)\boldsymbol{u}(\boldsymbol{y}) + \tfrac{1}{k^2}\textbf{grad}_{\boldsymbol{x}}\mathcal{G}(r;k)\text{div}_{\Gamma,y}\boldsymbol{u}(\boldsymbol{y})\right] d\boldsymbol{y}\right),\\
\mathbf{f}[\boldsymbol{x};\boldsymbol{\mu}] &= -\gamma_t\left(\boldsymbol{E}^{\text{inc}}(\boldsymbol{x};\boldsymbol{\mu})\right),
\end{aligned}$$

with $\gamma_t(\boldsymbol{u}) = \boldsymbol{n}\times(\boldsymbol{u}\times\boldsymbol{n})$ on Γ. The EFIE can be cast in terms of a variational problem: for a given parameter value $\boldsymbol{\mu} \in \boldsymbol{\mathcal{P}}$, find $\boldsymbol{u}(\boldsymbol{\mu}) \in \boldsymbol{X} := \boldsymbol{H}_{\text{div}}^{-\frac{1}{2}}(\Gamma)$ such that

$$a[\boldsymbol{u}(\boldsymbol{\mu}), \boldsymbol{v}; \boldsymbol{\mu}] = f[\boldsymbol{v};\boldsymbol{\mu}] \tag{2.5}$$

for all $\boldsymbol{v} \in \boldsymbol{X}$. The sesquilinear and linear forms are given by

$$\begin{aligned}
a[\boldsymbol{u},\boldsymbol{v};\boldsymbol{\mu}] &= ikZ\int_{\Gamma\times\Gamma} \mathcal{G}(r;k)\boldsymbol{u}(\boldsymbol{y})\cdot\overline{\boldsymbol{v}(\boldsymbol{x})}\, d\boldsymbol{y}\, d\boldsymbol{x}\\
&\quad - \tfrac{iZ}{k}\int_{\Gamma\times\Gamma} \mathcal{G}(r;k)\text{div}_{\Gamma,y}\boldsymbol{u}(\boldsymbol{y})\text{div}_{\Gamma,x}\overline{\boldsymbol{v}(\boldsymbol{x})}\, d\boldsymbol{y}\, d\boldsymbol{x},\\
f[\boldsymbol{v};\boldsymbol{\mu}] &= -\int_\Gamma \boldsymbol{E}^{\text{inc}}(\boldsymbol{x};\boldsymbol{\mu})\cdot\overline{\boldsymbol{v}(\boldsymbol{x})}\, d\boldsymbol{x}.
\end{aligned}$$

Here and in the following that we use $\boldsymbol{u}$ instead of $\boldsymbol{u}(\boldsymbol{\mu})$ at times for sake of simple presentation. Note that projecting $\boldsymbol{E}^{\text{inc}}(\boldsymbol{x};\boldsymbol{\mu})$ onto the surface Γ is no more necessary since $\boldsymbol{v}$ is a tangential function.

Let $\mathcal{T}_h$ be a family of shape-regular triangulations decomposing Γ into flat triangles. By $\boldsymbol{RT}_0(T)$ we denote the local Raviart-Thomas space on Γ of complex-valued functions on $T \in \mathcal{T}_h$ defined by (cf. [12])

$$\boldsymbol{RT}_0(T) := \left\{ \boldsymbol{v}_h(\boldsymbol{x}) = \boldsymbol{\alpha} + \beta \boldsymbol{x} \,\middle|\, \boldsymbol{\alpha} \in \mathbb{C}^2, \beta \in \mathbb{C}, \boldsymbol{x} \in T \right\}.$$

On a global level, the Raviart-Thomas space is defined by

$$\boldsymbol{RT}_0 := \left\{ \boldsymbol{v}_h \in \boldsymbol{H}^0_{\text{div}}(\Gamma) \,\middle|\, \boldsymbol{v}_h|_T \in \boldsymbol{RT}_0(T) \quad \forall T \in \mathcal{T}_h \right\},$$

where $\boldsymbol{H}^0_{\text{div}}(\Gamma)$ is defined in a standard manner

$$\boldsymbol{H}^0_{\text{div}}(\Gamma) := \left\{ \boldsymbol{v} \in \boldsymbol{L}^2_t(\Gamma) \,\middle|\, \text{div}_\Gamma \boldsymbol{v} \in L^2(\Gamma) \right\}.$$

Observe that the approximation space is conforming, i.e. $\boldsymbol{RT}_0 \subset \boldsymbol{H}^0_{\text{div}}(\Gamma) \subset \boldsymbol{H}^{-\frac{1}{2}}_{\text{div}}(\Gamma)$.

The corresponding boundary element method then consists of seeking, for any given parameter value $\boldsymbol{\mu} \in \boldsymbol{\mathcal{P}}$, the discrete solution $\boldsymbol{u}_h(\boldsymbol{\mu}) \in \boldsymbol{X}_h$ such that

$$a[\boldsymbol{u}_h(\boldsymbol{\mu}), \boldsymbol{v}_h; \boldsymbol{\mu}] = f[\boldsymbol{v}_h; \boldsymbol{\mu}], \tag{2.6}$$

for all $\boldsymbol{v}_h \in \boldsymbol{X}_h$.

For different configurations defined by a particular value of the parameter $\boldsymbol{\mu} = (k, \hat{\boldsymbol{d}}, \hat{\boldsymbol{p}}) \in \boldsymbol{\mathcal{P}}$ we are interested in studying the the radar cross section (RCS) of D, measured by a receiver situated in the direction $\hat{\boldsymbol{d}}_0 \in \mathbb{S}^2$. We denote the set of parameters for the output functional by $\boldsymbol{\mu}_s \in \boldsymbol{\mathcal{P}_s}$ for some parameter domain $\boldsymbol{\mathcal{P}_s} \subset \mathbb{R}^+ \times \mathbb{S}^2$. It contains the wave-number k and some directional unit vector $\hat{\boldsymbol{d}}_0 \in \mathbb{S}^2$.

The RCS is an indication of the directional far field associated with a scatterer D. It is a functional of the electric current $\boldsymbol{u}(\boldsymbol{\mu})$ on the surface and is defined by

$$\text{rcs}[\boldsymbol{u}(\boldsymbol{\mu}); \boldsymbol{\mu}, \boldsymbol{\mu}_s] := 10 \log_{10} \left(4\pi \frac{|\boldsymbol{s}_\infty[\boldsymbol{u}(\boldsymbol{\mu}); \boldsymbol{\mu}_s]|^2}{|\boldsymbol{E}^{\text{inc}}(\boldsymbol{\mu})|^2} \right)$$

where $\boldsymbol{s}_\infty$ is a linear functional of $\boldsymbol{u}(\boldsymbol{\mu})$ given by

$$\boldsymbol{s}_\infty[\boldsymbol{u}(\boldsymbol{\mu}); \boldsymbol{\mu}_s] := \frac{ikZ}{4\pi} \int_\Gamma \hat{\boldsymbol{d}}_0 \times (\boldsymbol{u}(\boldsymbol{x}; \boldsymbol{\mu}) \times \hat{\boldsymbol{d}}_0) e^{ik\boldsymbol{x} \cdot \hat{\boldsymbol{d}}_0} \, d\boldsymbol{x}.$$

The RCS represents the energy of the total electric field $\boldsymbol{E}$ at infinity in the direction $\hat{\boldsymbol{d}}_0$.

2.2. Introduction to the Reduced Basis Method. For parametrized scattering problems we are interested in a fast evaluation of the following input-output procedure:

$$\boldsymbol{\mu} \in \boldsymbol{\mathcal{P}} \quad \longrightarrow \quad \text{solve: } L_h[\boldsymbol{u}_h(\boldsymbol{\mu}); \boldsymbol{\mu}] = 0 \quad \longrightarrow \quad \text{rcs}[\boldsymbol{u}_h(\boldsymbol{\mu}); \boldsymbol{\mu}, \boldsymbol{\mu}_s] \tag{2.7}$$

where solving $L_h[\boldsymbol{u}_h(\boldsymbol{\mu}); \boldsymbol{\mu}] = 0$ schematically represents solving problem (2.6). We refer to this procedure as the *truth solver*.

We consider problems where the output functional $\text{rcs}\,[\boldsymbol{u}_h(\boldsymbol{\mu}); \boldsymbol{\mu}, \boldsymbol{\mu}_s]$ needs to be computed for many different parameter values $\boldsymbol{\mu}$. In this case, solving the full

boundary element problem each new parameter value is not a viable option. The Reduced Basis Method is an algorithmic completion of the boundary element method to solve in a fast manner

$$\boldsymbol{\mu} \in \boldsymbol{\mathcal{P}} \quad \longrightarrow \quad \text{solve: } L_N[\boldsymbol{u}_N(\boldsymbol{\mu}); \boldsymbol{\mu}] = 0 \quad \longrightarrow \quad \text{rcs}[\boldsymbol{u}_N(\boldsymbol{\mu}); \boldsymbol{\mu}, \boldsymbol{\mu}_s]. \tag{2.8}$$

The reduced basis space approximates the discrete space

$$\boldsymbol{X}_N \approx \{\boldsymbol{u}_h(\boldsymbol{\mu}) \,:\, \boldsymbol{\mu} \in \boldsymbol{\mathcal{P}}\}.$$

and accuracy of scheme is controlled by the quality of this approximation. We denote the dimension of $\boldsymbol{X}_N$ by N and the dimension of the boundary element space $\boldsymbol{X}_h$ by $\mathcal{N}$. Solving $L_N[\boldsymbol{u}_N(\boldsymbol{\mu}); \boldsymbol{\mu}] = 0$ consists of: for any given parameter value $\boldsymbol{\mu} \in \boldsymbol{\mathcal{P}}$, the discrete solution $\boldsymbol{u}_N(\boldsymbol{\mu}) \in \boldsymbol{X}_N$ such that

$$a[\boldsymbol{u}_N(\boldsymbol{\mu}), \boldsymbol{v}_N; \boldsymbol{\mu}] = f[\boldsymbol{v}_N; \boldsymbol{\mu}], \tag{2.9}$$

for all $\boldsymbol{v}_N \in \boldsymbol{X}_N$. The complexity of this problem depends then on N and is independent of $\mathcal{N}$. Empirically, for the problems under consideration one can observe that $N \ll \mathcal{N}$, making it clear that there is a substantial advantage in solving the Reduced Basis problem $L_N[\boldsymbol{u}_N(\boldsymbol{\mu}); \boldsymbol{\mu}] = 0$ as it is much faster than solving the boundary element problem However, the remaining questions are

- How to find basis functions for $\boldsymbol{X}_N$?
- How to solve (2.9) efficiently?

The common approach for reduced basis methods is to build $\boldsymbol{X}_N$ as the span of solution to (2.6) for particular parameter values (called *snapshots*), i.e.,

$$\boldsymbol{X}_N = \text{span}\{\boldsymbol{u}_h(\boldsymbol{\mu}_1), \ldots, \boldsymbol{u}_h(\boldsymbol{\mu}_N)\},$$

where $\boldsymbol{\mu}_1, \ldots, \boldsymbol{\mu}_N$ are selectively chosen parameters. Those sample points are selected using a Greedy algorithm [] to optimize cost and accuracy. Given an error indicator $\eta(\boldsymbol{\mu}) \approx \|\boldsymbol{u}_h(\boldsymbol{\mu}) - \boldsymbol{u}_N(\boldsymbol{\mu})\|_{\boldsymbol{X}_h}$ to indicate the error of the reduced basis approximation of (2.9) with respect to the boundary element solution (2.6) (the *truth solution*) in a given norm $\|\cdot\|_{\boldsymbol{X}_h}$, we proceed as follows

`0:` Pick arbitrarily $\boldsymbol{\mu}_1 \in \boldsymbol{\mathcal{P}}$, set $N = 1$ and $W_0 = \emptyset$.

`1:` Solve $L_h(\boldsymbol{u}_h(\boldsymbol{\mu}_N); \boldsymbol{\mu}_N) = 0$, set $W_N = \text{span}\{W_{N-1}, \boldsymbol{u}_h(\boldsymbol{\mu}_N)\}$.

`2:` Consider the procedure

$$\boldsymbol{\mu} \in \boldsymbol{\mathcal{P}} \quad \longrightarrow \quad \text{solve: } L_N(\boldsymbol{u}_N(\boldsymbol{\mu}); \boldsymbol{\mu}) = 0 \quad \longrightarrow \quad \eta(\boldsymbol{\mu})$$

and find $\boldsymbol{\mu}_{N+1} = \arg\max_{\boldsymbol{\mu} \in \boldsymbol{\mathcal{P}}} \eta(\boldsymbol{\mu})$.

`3:` Set $N := N + 1$ and go to `1`.

This procedure is applied until $\max_{\boldsymbol{\mu} \in \boldsymbol{\mathcal{P}}} \eta(\boldsymbol{\mu})$ is small enough or a maximum of iterations is attained. In this manner, we construct an N-dimensional reduced basis space by only solving N boundary element problems. In addition, we obtain a hierarchical basis.

In order to only select the necessary modes, it is important that the error estimate $\eta(\boldsymbol{\mu})$ is as accurate as possible. In addition, if the estimate is such that

$$\eta(\boldsymbol{\mu}) \geq \|\boldsymbol{u}_h(\boldsymbol{\mu}) - \boldsymbol{u}_N(\boldsymbol{\mu})\|_{\boldsymbol{X}_h}$$

and the computable error estimate guarantees that $\eta(\boldsymbol{\mu}) \leq \texttt{Tol}$ for all parameter values, then a minimal error tolerance of $\|\boldsymbol{u}_h(\boldsymbol{\mu}) - \boldsymbol{u}_N(\boldsymbol{\mu})\|_{\boldsymbol{X}_h} \leq \texttt{Tol}$ can be *certified*. For more details, see the upcoming Section 3.1.

The second point requires attention on how to solve $L_N[\boldsymbol{u}_N(\boldsymbol{\mu}); \boldsymbol{\mu}] = 0$ resp. (2.9) efficiently. As stated earlier, problem (2.9) can be written as a N-dimensional linear system

$$\mathbf{A}(\boldsymbol{\mu})\, \boldsymbol{U}_N(\boldsymbol{\mu}) = \mathbf{F}(\boldsymbol{\mu}),$$

where $\mathbf{A}(\boldsymbol{\mu})$ is the matrix corresponding to the sesquilinear form $a[\cdot, \cdot; \boldsymbol{\mu}]$ and $\mathbf{F}(\boldsymbol{\mu})$ is the vector corresponding to the linear form $f[\cdot; \boldsymbol{\mu}]$ whereas $\boldsymbol{U}_N(\boldsymbol{\mu})$ is the solution vector, i.e. the representation of $\boldsymbol{u}_N(\boldsymbol{\mu})$ in a chosen basis of $\boldsymbol{X}_N$. This is an N-dimensional system. Thus, solving it does not depend on the dimension $\mathcal{N}$ of the underlying boundary element space $\boldsymbol{X}_h$. However, assembling the matrix $\mathbf{A}(\boldsymbol{\mu})$ does depend on $\mathcal{N}$. Since one is interested in computing the reduced basis solution for many different parameter values, it is important to satisfy the following affine decomposition property

$$a[\boldsymbol{u}, \boldsymbol{v}; \boldsymbol{\mu}] = \sum_{q=1}^{Q_{\mathtt{a}}} \theta_{\mathtt{a}}^q(\boldsymbol{\mu})\, a^q[\boldsymbol{u}, \boldsymbol{v}], \tag{2.10}$$

$$f[\boldsymbol{v}; \boldsymbol{\mu}] = \sum_{q=1}^{Q_{\mathtt{f}}} \theta_{\mathtt{f}}^q(\boldsymbol{\mu})\, f^q[\boldsymbol{v}], \tag{2.11}$$

$$\boldsymbol{s}_\infty[\boldsymbol{u}, \boldsymbol{\mu}_s] = \sum_{q=1}^{Q_{\infty,m}} \theta_{\infty,\mathtt{m}}^q(\boldsymbol{\mu})\, \boldsymbol{s}_\infty^q[\boldsymbol{u}]. \tag{2.12}$$

Thus we impose a separation of parameter dependent scalar functions $\theta_{\mathtt{a}}^q$, $\theta_{\mathtt{f}}^q$, $\theta_{\infty,\mathtt{m}}^q$ and parameter independent forms a^q, f^q, $\boldsymbol{s}_\infty^q$. This assumption allows for an offline/online separation where, during the offline phase we compute the reduced basis and assemble the parameter independent $N \times N$-dimensional matrices $\mathbf{A}^q$, and the N-dimensional vectors $\mathbf{F}^q$, $\boldsymbol{S}_\infty^q$.

During the online procedure (2.8) then takes the following form: For any new parameter value $\boldsymbol{\mu} \in \boldsymbol{\mathcal{P}}$, assemble the matrix and vector

$$\boldsymbol{A}(\boldsymbol{\mu}) = \sum_{q=1}^{Q_{\mathtt{a}}} \theta_{\mathtt{a}}^q(\boldsymbol{\mu})\, \mathbf{A}^q,$$

$$\boldsymbol{F}(\boldsymbol{\mu}) = \sum_{q=1}^{Q_{\mathtt{f}}} \theta_{\mathtt{f}}^q(\boldsymbol{\mu})\, \mathbf{F}^q,$$

$$\boldsymbol{S}_\infty(\boldsymbol{\mu}_s) = \sum_{q=1}^{Q_{\infty,m}} \theta_{\infty,\mathtt{m}}^q(\boldsymbol{\mu}_s)\, \boldsymbol{S}_\infty^q,$$

solve the linear system

$$\boldsymbol{A}(\boldsymbol{\mu})\, \boldsymbol{U}_N(\boldsymbol{\mu}) = \boldsymbol{F}(\boldsymbol{\mu})$$

and compute the RCS-signature

$$\begin{aligned} \boldsymbol{s}_\infty[\boldsymbol{u}_N(\boldsymbol{\mu}), \boldsymbol{\mu}_s] &= \boldsymbol{S}_\infty(\boldsymbol{\mu}_s)\, \boldsymbol{U}_N(\boldsymbol{\mu}) (\text{ to check dimensions etc}) \\ \mathrm{rcs}[\boldsymbol{u}_N(\boldsymbol{\mu}), \boldsymbol{\mu}, \boldsymbol{\mu}_s] &= 10 \log_{10} \left(4\pi \frac{|\boldsymbol{s}_\infty[\boldsymbol{u}(\boldsymbol{\mu}); \boldsymbol{\mu}_s]|^2}{|\boldsymbol{E}^{\mathrm{inc}}(\boldsymbol{\mu})|^2} \right). \end{aligned}$$

Observe that the online procedure is independent of $\mathcal{N}$ and, thus, can be computed at very limited computational cost.

Observe that the affine decomposition can not be satisfied in an exact manner for the sesequilinear and linear forms $a[\cdot, \cdot; \boldsymbol{\mu}]$, $f[\cdot; \boldsymbol{\mu}]$ and $\boldsymbol{s}_\infty[\cdot; \boldsymbol{\mu}_s]$. This can be overcome by using the Empirical Interpolation Method (EIM) to satisfy the condition in an approximative manner to any desired tolerance. For more informations on how to apply to the EIM we refer to [5, Section 5] for a detailed discussion.

3. Certified online error estimation. Having discussed the core elements of the algorithm above, let us in the following develop the a posteriori error estimator and discuss its implementation in an online manner that allows for a fast and accurate evaluation of the estimator to certify the accuracy of the output of interest.

3.1. Certified a posteriori estimation. The goal of this section is to construct the a posterior error indicator $\eta(\boldsymbol{\mu})$, required during the greedy construction to assemble the reduced basis and during the online procedure to certify a certain error tolerance of the error

$$\|\boldsymbol{u}_h(\boldsymbol{\mu}) - \boldsymbol{u}_N(\boldsymbol{\mu})\|_{\boldsymbol{X}_h},$$

where $\|\cdot\|_{\boldsymbol{X}_h}$ is a suitable norm for $\boldsymbol{X}_h$ with scalar product $(\cdot, \cdot)_{\boldsymbol{X}_h}$. Let $\boldsymbol{e}(\boldsymbol{\mu}) = \boldsymbol{u}_h(\boldsymbol{\mu}) - \boldsymbol{u}_N(\boldsymbol{\mu}) \in \boldsymbol{X}_h$ be the error function satisfying

$$a[\boldsymbol{e}(\boldsymbol{\mu}), \boldsymbol{v}_h; \boldsymbol{\mu}] = r[\boldsymbol{v}_h; \boldsymbol{\mu}], \qquad \forall \boldsymbol{v}_h \in \boldsymbol{X}_h$$

where $r[\cdot; \boldsymbol{\mu}] \in \boldsymbol{X}_h'$ is the residual

$$r[\boldsymbol{v}_h; \boldsymbol{\mu}] = \boldsymbol{f}[\boldsymbol{v}_h; \boldsymbol{\mu}] - a[\boldsymbol{u}_N(\boldsymbol{\mu}), \boldsymbol{v}_h; \boldsymbol{\mu}], \qquad \forall \boldsymbol{v}_h \in \boldsymbol{X}_h.$$

Referring to its Riesz representation $\hat{\boldsymbol{e}}(\boldsymbol{\mu}) \in \boldsymbol{X}_h$ yields

$$(\hat{\boldsymbol{e}}(\boldsymbol{\mu}), \boldsymbol{v}_h)_{\boldsymbol{X}_h} = r[\boldsymbol{v}_h; \boldsymbol{\mu}], \qquad \forall \boldsymbol{v}_h \in \boldsymbol{X}_h,$$

and thus

$$a[\boldsymbol{e}(\boldsymbol{\mu}), \boldsymbol{v}_h; \boldsymbol{\mu}] = (\hat{\boldsymbol{e}}(\boldsymbol{\mu}), \boldsymbol{v}_h)_{\boldsymbol{X}_h}. \tag{3.1}$$

In addition, by definition of the operator norm we have

$$\|r[\cdot; \boldsymbol{\mu}]\|_{\boldsymbol{X}_h'} = \sup_{\boldsymbol{v}_h \in \boldsymbol{X}_h} \frac{r[\boldsymbol{v}_h; \boldsymbol{\mu}]}{\|\boldsymbol{v}_h\|_{\boldsymbol{X}_h}} = \|\hat{\boldsymbol{e}}(\boldsymbol{\mu})\|_{\boldsymbol{X}_h}.$$

Under the assumption that (2.9) is uniquely solvable, the following holds: for each $\boldsymbol{\mu} \in \boldsymbol{\mathcal{P}}$, there exists an $\beta_h(\boldsymbol{\mu}) > 0$ such that

$$\beta_h(\boldsymbol{\mu}) \|\boldsymbol{v}_h\|_{\boldsymbol{X}_h} \leq \sup_{\boldsymbol{w}_h \in \boldsymbol{X}_h} \frac{a[\boldsymbol{v}_h, \boldsymbol{w}_h; \boldsymbol{\mu}]}{\|\boldsymbol{w}_h\|_{\boldsymbol{X}_h}}, \qquad \forall \boldsymbol{v}_h \in \boldsymbol{X}_h. \tag{3.2}$$

Now, assuming that we can easily, and independently of $\mathcal{N}$, compute a lower bound $0 < \beta_{\mathtt{LB}}(\boldsymbol{\mu}) \leq \beta_h(\boldsymbol{\mu})$, for any $\boldsymbol{\mu} \in \boldsymbol{\mathcal{P}}$, we define the a posteriori estimate as

$$\eta_N(\boldsymbol{\mu}) = \frac{\|\hat{\boldsymbol{e}}(\boldsymbol{\mu})\|_{\boldsymbol{X}_h}}{\beta_{\mathtt{LB}}(\boldsymbol{\mu})}. \tag{3.3}$$

PROPOSITION 3.1. *[11] The a posteriori estimator defined in (3.3) is reliable, i.e.,*

$$\|\boldsymbol{u}_h(\boldsymbol{\mu}) - \boldsymbol{u}_N(\boldsymbol{\mu})\|_{\boldsymbol{X}_h} \leq \eta_N(\boldsymbol{\mu}).$$

Proof. Indeed, combining the inf-sup condition(3.2) with (3.1) yields

$$\beta_h(\boldsymbol{\mu})\, \|\boldsymbol{e}(\boldsymbol{\mu})\|_{\boldsymbol{X}_h} \leq \sup_{\boldsymbol{w}_h \in \boldsymbol{X}_h} \frac{a[\boldsymbol{e}(\boldsymbol{\mu}), \boldsymbol{w}_h; \boldsymbol{\mu}]}{\|\boldsymbol{w}_h\|_{\boldsymbol{X}_h}} = \sup_{\boldsymbol{w}_h \in \boldsymbol{X}_h} \frac{(\hat{\boldsymbol{e}}(\boldsymbol{\mu}), \boldsymbol{w}_h)_{\boldsymbol{X}_h}}{\|\boldsymbol{w}_h\|_{\boldsymbol{X}_h}} \leq \|\hat{\boldsymbol{e}}(\boldsymbol{\mu})\|_{\boldsymbol{X}_h}$$

and thus

$$\|\boldsymbol{e}(\boldsymbol{\mu})\|_{\boldsymbol{X}_h} \leq \tfrac{1}{\beta_h(\boldsymbol{\mu})} \|\hat{\boldsymbol{e}}(\boldsymbol{\mu})\|_{\boldsymbol{X}_h} \leq \tfrac{1}{\beta_{\mathtt{LB}}(\boldsymbol{\mu})} \|\hat{\boldsymbol{e}}(\boldsymbol{\mu})\|_{\boldsymbol{X}_h} = \eta_N(\boldsymbol{\mu}).$$

□ Under the condition, that for the given norm $\|\cdot\|_{\boldsymbol{X}_h}$, the form $a[\cdot, \cdot; \boldsymbol{\mu}]$ is also continuous, that is: for each $\boldsymbol{\mu} \in \boldsymbol{\mathcal{P}}$, there exists a constant $\gamma_h(\boldsymbol{\mu}) > 0$ such that

$$a[\boldsymbol{v}_h, \boldsymbol{w}_h; \boldsymbol{\mu}] \leq \gamma_h(\boldsymbol{\mu})\, \|\boldsymbol{v}_h\|_{\boldsymbol{X}_h} \|\boldsymbol{w}_h\|_{\boldsymbol{X}_h}, \qquad \forall \boldsymbol{v}_h, \boldsymbol{w}_h \in \boldsymbol{X}_h,$$

one can prove the following efficiency result:

PROPOSITION 3.2. *The a posteriori estimator defined in (3.3) is efficient, i.e.,*

$$\eta_N(\boldsymbol{\mu}) \leq \tfrac{\gamma_h(\boldsymbol{\mu})}{\beta_{\mathtt{LB}}(\boldsymbol{\mu})} \|\boldsymbol{e}(\boldsymbol{\mu})\|_{\boldsymbol{X}_h}.$$

Proof. Given that

$$\|\hat{\boldsymbol{e}}(\boldsymbol{\mu})\|^2_{\boldsymbol{X}_h} = a[\boldsymbol{e}(\boldsymbol{\mu}), \hat{\boldsymbol{e}}(\boldsymbol{\mu}); \boldsymbol{\mu}] \leq \gamma_h(\boldsymbol{\mu})\, \|\boldsymbol{e}(\boldsymbol{\mu})\|_{\boldsymbol{X}_h}\, \|\hat{\boldsymbol{e}}(\boldsymbol{\mu})\|_{\boldsymbol{X}_h}$$

we conclude that

$$\eta_N(\boldsymbol{\mu}) = \tfrac{1}{\beta_{\mathtt{LB}}(\boldsymbol{\mu})} \|\hat{\boldsymbol{e}}(\boldsymbol{\mu})\|_{\boldsymbol{X}_h} \leq \tfrac{\gamma_h(\boldsymbol{\mu})}{\beta_{\mathtt{LB}}(\boldsymbol{\mu})} \|\boldsymbol{e}(\boldsymbol{\mu})\|_{\boldsymbol{X}_h}.$$

□

PROPOSITION 3.3. *The error in the output functional $\boldsymbol{s}_\infty$ is certified by the following computable error bound*

$$|\boldsymbol{s}_\infty[\boldsymbol{u}_h(\boldsymbol{\mu}); \boldsymbol{\mu}_s] - \boldsymbol{s}_\infty[\boldsymbol{u}_N(\boldsymbol{\mu}); \boldsymbol{\mu}_s]| < \tfrac{kZ|\Gamma|^{\frac{1}{2}}}{4\pi} \eta_N(\boldsymbol{\mu}).$$

Proof. By linearity of $\boldsymbol{s}_\infty$ and Proposition 3.1, observe that the following bound holds

$$\begin{aligned} |\boldsymbol{s}_\infty[\boldsymbol{u}_h(\boldsymbol{\mu}); \boldsymbol{\mu}_s] - \boldsymbol{s}_\infty[\boldsymbol{u}_N(\boldsymbol{\mu}); \boldsymbol{\mu}_s]| = \boldsymbol{s}_\infty[\boldsymbol{u}_h(\boldsymbol{\mu}) - \boldsymbol{u}_N(\boldsymbol{\mu}); \boldsymbol{\mu}_s]| &\leq \|s_\infty[\cdot; k, \hat{\boldsymbol{d}}_0]\|_{\boldsymbol{X}_h'}\, \|\boldsymbol{u}_h(\boldsymbol{\mu}) - \boldsymbol{u}_N(\boldsymbol{\mu})\|_{\boldsymbol{X}_h} \\ &\leq \|s_\infty[\cdot; k, \hat{\boldsymbol{d}}_0]\|_{\boldsymbol{X}_h'}\, \eta_N(\boldsymbol{\mu}), \end{aligned}$$

where the operator norm can be estimated by

$$\begin{aligned}\|s_\infty[\cdot;k,\hat{\boldsymbol{d}}_0]\|_{\boldsymbol{X}_h'} &= \sup_{\boldsymbol{w}_h\in\boldsymbol{X}_h}\frac{|s_\infty[\boldsymbol{w}_h;k,\hat{\boldsymbol{d}}_0]|}{\|\boldsymbol{w}_h\|_{\boldsymbol{X}_h}} = \frac{kZ}{4\pi}\sup_{\boldsymbol{w}_h\in\boldsymbol{X}_h}\frac{|\int_\Gamma \hat{\boldsymbol{d}}_0\times(\boldsymbol{w}_h(\boldsymbol{x};\boldsymbol{\mu})\times\hat{\boldsymbol{d}}_0)e^{ik\boldsymbol{x}\cdot\hat{\boldsymbol{d}}_0}\,d\boldsymbol{x}|}{\|\boldsymbol{w}_h\|_{\boldsymbol{X}_h}}\\ &\le \frac{kZ}{4\pi}\sup_{\boldsymbol{w}_h\in\boldsymbol{X}_h}\frac{|\int_\Gamma \boldsymbol{w}_h(\boldsymbol{x};\boldsymbol{\mu})e^{ik\boldsymbol{x}\cdot\hat{\boldsymbol{d}}_0}\,d\boldsymbol{x}|}{\|\boldsymbol{w}_h\|_{\boldsymbol{X}_h}} \le \frac{kZ}{4\pi}\sup_{\boldsymbol{w}_h\in\boldsymbol{X}_h}\frac{\|\boldsymbol{w}_h\|_{L^2(\Gamma)}\|1\|_{L^2(\Gamma)}}{\|\boldsymbol{w}_h\|_{\boldsymbol{X}_h}}\\ &= \frac{kZ|\Gamma|^{\frac{1}{2}}}{4\pi}\sup_{\boldsymbol{w}_h\in\boldsymbol{X}_h}\frac{\|\boldsymbol{w}_h\|_{L^2(\Gamma)}}{\|\boldsymbol{w}_h\|_{\boldsymbol{X}_h}} \le \frac{kZ|\Gamma|^{\frac{1}{2}}}{4\pi}.\end{aligned}$$

□

COROLLARY 3.4. *Given $\boldsymbol{s}_\infty[\boldsymbol{u}_N(\boldsymbol{\mu});\boldsymbol{\mu}_s]$ and the error certification $\varepsilon_s = \frac{kZ|\Gamma|^{\frac{1}{2}}}{4\pi}\eta_N(\boldsymbol{\mu})$, the truth functional $\boldsymbol{s}_\infty[\boldsymbol{u}_h(\boldsymbol{\mu});\boldsymbol{\mu}_s]$ lies within the error bars*

$$\boldsymbol{s}_\infty[\boldsymbol{u}_N(\boldsymbol{\mu});\boldsymbol{\mu}_s] - \varepsilon_s \le \boldsymbol{s}_\infty[\boldsymbol{u}_h(\boldsymbol{\mu});\boldsymbol{\mu}_s] \le \boldsymbol{s}_\infty[\boldsymbol{u}_N(\boldsymbol{\mu});\boldsymbol{\mu}_s] + \varepsilon_s.$$

PROPOSITION 3.5. *The error in the radar cross section* rcs *is certified by the following computable error bound*

$$\begin{aligned}&|\mathrm{rcs}[\boldsymbol{u}_h(\boldsymbol{\mu});\boldsymbol{\mu},\boldsymbol{\mu}_s] - \mathrm{rcs}[\boldsymbol{u}_N(\boldsymbol{\mu});\boldsymbol{\mu},\boldsymbol{\mu}_s]|\\ &\qquad\le 20\max\left(\log_{10}\left(\frac{|\boldsymbol{s}_\infty[\boldsymbol{u}_N(\boldsymbol{\mu});\boldsymbol{\mu}_s]| + \varepsilon_s}{|\boldsymbol{s}_\infty[\boldsymbol{u}_N(\boldsymbol{\mu});\boldsymbol{\mu}_s]|}\right), \log_{10}\left(\frac{|\boldsymbol{s}_\infty[\boldsymbol{u}_N(\boldsymbol{\mu});\boldsymbol{\mu}_s]|}{|\boldsymbol{s}_\infty[\boldsymbol{u}_N(\boldsymbol{\mu});\boldsymbol{\mu}_s]| - \varepsilon_s}\right)\right).\end{aligned}$$

Proof. Using properties of the logarithmic function, note that

$$\begin{aligned}&\mathrm{rcs}[\boldsymbol{u}_h(\boldsymbol{\mu});\boldsymbol{\mu},\boldsymbol{\mu}_s] - \mathrm{rcs}[\boldsymbol{u}_N(\boldsymbol{\mu});\boldsymbol{\mu},\boldsymbol{\mu}_s]\\ &\qquad= 10\left(\log_{10}\left(4\pi\frac{|\boldsymbol{s}_\infty[\boldsymbol{u}_h(\boldsymbol{\mu});\boldsymbol{\mu}_s]|^2}{|\boldsymbol{E}^{\mathrm{inc}}(\boldsymbol{\mu})|^2}\right) - \log_{10}\left(4\pi\frac{|\boldsymbol{s}_\infty[\boldsymbol{u}_N(\boldsymbol{\mu});\boldsymbol{\mu}_s]|^2}{|\boldsymbol{E}^{\mathrm{inc}}(\boldsymbol{\mu})|^2}\right)\right)\\ &\qquad= 20\left(\log_{10}\left(|\boldsymbol{s}_\infty[\boldsymbol{u}_h(\boldsymbol{\mu});\boldsymbol{\mu}_s]|\right) - \log_{10}\left(|\boldsymbol{s}_\infty[\boldsymbol{u}_N(\boldsymbol{\mu});\boldsymbol{\mu}_s]|\right)\right)\\ &\qquad= 20\log_{10}\left(\frac{|\boldsymbol{s}_\infty[\boldsymbol{u}_h(\boldsymbol{\mu});\boldsymbol{\mu}_s]|}{|\boldsymbol{s}_\infty[\boldsymbol{u}_N(\boldsymbol{\mu});\boldsymbol{\mu}_s]|}\right).\end{aligned}$$

From the bound

$$|\boldsymbol{s}_\infty[\boldsymbol{u}_h(\boldsymbol{\mu});\boldsymbol{\mu}_s] - \boldsymbol{s}_\infty[\boldsymbol{u}_N(\boldsymbol{\mu});\boldsymbol{\mu}_s]| < \varepsilon_s$$

and using the inverse triangle inequality we deduce the error bars

$$|\boldsymbol{s}_\infty[\boldsymbol{u}_N(\boldsymbol{\mu});\boldsymbol{\mu}_s]| - \varepsilon_s < |\boldsymbol{s}_\infty[\boldsymbol{u}_h(\boldsymbol{\mu});\boldsymbol{\mu}_s]| < |\boldsymbol{s}_\infty[\boldsymbol{u}_N(\boldsymbol{\mu});\boldsymbol{\mu}_s]| + \varepsilon_s$$

and

$$\frac{|\boldsymbol{s}_\infty[\boldsymbol{u}_N(\boldsymbol{\mu});\boldsymbol{\mu}_s]| - \varepsilon_s}{|\boldsymbol{s}_\infty[\boldsymbol{u}_N(\boldsymbol{\mu});\boldsymbol{\mu}_s]|} < \frac{|\boldsymbol{s}_\infty[\boldsymbol{u}_h(\boldsymbol{\mu});\boldsymbol{\mu}_s]|}{|\boldsymbol{s}_\infty[\boldsymbol{u}_N(\boldsymbol{\mu});\boldsymbol{\mu}_s]|} < \frac{|\boldsymbol{s}_\infty[\boldsymbol{u}_N(\boldsymbol{\mu});\boldsymbol{\mu}_s]| + \varepsilon_s}{|\boldsymbol{s}_\infty[\boldsymbol{u}_N(\boldsymbol{\mu});\boldsymbol{\mu}_s]|}.$$

Thus, we get the bounds

$$\frac{|\boldsymbol{s}_\infty[\boldsymbol{u}_h(\boldsymbol{\mu});\boldsymbol{\mu}_s]|}{|\boldsymbol{s}_\infty[\boldsymbol{u}_N(\boldsymbol{\mu});\boldsymbol{\mu}_s]|} < \frac{|\boldsymbol{s}_\infty[\boldsymbol{u}_N(\boldsymbol{\mu});\boldsymbol{\mu}_s]| + \varepsilon_s}{|\boldsymbol{s}_\infty[\boldsymbol{u}_N(\boldsymbol{\mu});\boldsymbol{\mu}_s]|} \qquad \text{and} \qquad \frac{|\boldsymbol{s}_\infty[\boldsymbol{u}_N(\boldsymbol{\mu});\boldsymbol{\mu}_s]|}{|\boldsymbol{s}_\infty[\boldsymbol{u}_h(\boldsymbol{\mu});\boldsymbol{\mu}_s]|} < \frac{|\boldsymbol{s}_\infty[\boldsymbol{u}_N(\boldsymbol{\mu});\boldsymbol{\mu}_s]|}{|\boldsymbol{s}_\infty[\boldsymbol{u}_N(\boldsymbol{\mu});\boldsymbol{\mu}_s]| - \varepsilon_s},$$

and we can thus finally estimate

$$
\begin{aligned}
&|\mathrm{rcs}[\boldsymbol{u}_h(\boldsymbol{\mu});\boldsymbol{\mu},\boldsymbol{\mu}_s] - \mathrm{rcs}[\boldsymbol{u}_N(\boldsymbol{\mu});\boldsymbol{\mu},\boldsymbol{\mu}_s]| \\
&\qquad = 20\max\left(\log_{10}\left(\frac{|\boldsymbol{s}_\infty[\boldsymbol{u}_h(\boldsymbol{\mu});\boldsymbol{\mu}_s]|}{|\boldsymbol{s}_\infty[\boldsymbol{u}_N(\boldsymbol{\mu});\boldsymbol{\mu}_s]|}\right), \log_{10}\left(\frac{|\boldsymbol{s}_\infty[\boldsymbol{u}_N(\boldsymbol{\mu});\boldsymbol{\mu}_s]|}{|\boldsymbol{s}_\infty[\boldsymbol{u}_h(\boldsymbol{\mu});\boldsymbol{\mu}_s]|}\right)\right) \\
&\qquad \leq 20\max\left(\log_{10}\left(\frac{|\boldsymbol{s}_\infty[\boldsymbol{u}_N(\boldsymbol{\mu});\boldsymbol{\mu}_s]| + \varepsilon_s}{|\boldsymbol{s}_\infty[\boldsymbol{u}_N(\boldsymbol{\mu});\boldsymbol{\mu}_s]|}\right), \log_{10}\left(\frac{|\boldsymbol{s}_\infty[\boldsymbol{u}_N(\boldsymbol{\mu});\boldsymbol{\mu}_s]|}{|\boldsymbol{s}_\infty[\boldsymbol{u}_N(\boldsymbol{\mu});\boldsymbol{\mu}_s]| - \varepsilon_s}\right)\right).
\end{aligned}
$$

□

In our case, the intrinsic solution space $\boldsymbol{X}$ is the space $\boldsymbol{H}^{-\frac{1}{2}}(\mathrm{div}_\Gamma, \Gamma)$, see [7, 2], which induces a natural norm for the discrete space $\boldsymbol{X}_h$. Here the operator div_Γ denotes the surface divergence. This norm is however not computable in practice. Observing that the discrete approximation space $\boldsymbol{X}_h$ is a subspace of $\boldsymbol{H}(\mathrm{div}_\Gamma, \Gamma)$, we define the norm $\|\cdot\|_{\boldsymbol{X}_h}$ as

$$
\|\boldsymbol{v}_h\|^2_{\boldsymbol{X}_h} = \|\boldsymbol{v}_h\|^2_{L^2(\Gamma)} + \|\mathrm{div}_\Gamma \boldsymbol{v}_h\|^2_{L^2(\Gamma)}, \qquad \forall \boldsymbol{v}_h \in \boldsymbol{X}_h.
$$

In what follows, we shall use this norm to measure the error.

3.2. Efficient implementation of the error estimator. Under the assumption that the lower bound of the inf-sup constant is computable for any parameter value, independently of the dimension of the boundary element space $\mathcal{N}$, we show in this section how the error estimation $\eta(\boldsymbol{\mu})$ can be likewise be evaluated online independently of $\mathcal{N}$. The computation of the inf-sup constant is addressed in the upcoming Section 3.3.

Given the affine decompositions (2.10), (2.11) we write

$$
\begin{aligned}
(\hat{\boldsymbol{e}}(\boldsymbol{\mu}), \boldsymbol{v}_h)_{\boldsymbol{X}_h} = r[\boldsymbol{v}_h;\boldsymbol{\mu}] &= f[\boldsymbol{v}_h;\boldsymbol{\mu}] - a[\boldsymbol{u}_N(\boldsymbol{\mu}), \boldsymbol{v}_h;\boldsymbol{\mu}] \\
&= \sum_{q=1}^{Q_{\mathtt{f}}} \theta^q_{\mathtt{f}}(\boldsymbol{\mu})\, f^q[\boldsymbol{v}_h] - \sum_{q=1}^{Q_{\mathtt{a}}} \theta^q_{\mathtt{a}}(\boldsymbol{\mu})\, a^q[\boldsymbol{u}_N, \boldsymbol{v}_h] \\
&= \sum_{q=1}^{Q_{\mathtt{f}}} \theta^q_{\mathtt{f}}(\boldsymbol{\mu})\, f^q[\boldsymbol{v}_h] - \sum_{n=1}^{N}\sum_{q=1}^{Q_{\mathtt{a}}} u_n \theta^q_{\mathtt{a}}(\boldsymbol{\mu})\, a^q[\boldsymbol{\xi}_n, \boldsymbol{v}_h],
\end{aligned}
$$

where $\{\xi_n\}_{n=1}^N$ are basis functions of the reduced basis W_N and $\{u_n\}_{n=1}^N \subset \mathbb{C}$ the degrees of freedom with respect to $\{\xi_n\}_{n=1}^N$. Thus, we have

$$
\hat{\boldsymbol{e}}(\boldsymbol{\mu}) = \sum_{q=1}^{Q_{\mathtt{f}}} \theta^q_{\mathtt{f}}(\boldsymbol{\mu})\, \mathtt{f}^q - \sum_{n=1}^{N}\sum_{q=1}^{Q_{\mathtt{a}}} u_n \theta^q_{\mathtt{a}}(\boldsymbol{\mu})\, \mathtt{a}^{q,n}
$$

with $\mathtt{f}^q, \mathtt{a}^{q,n} \in \boldsymbol{X}_h$ such that

$$
\begin{aligned}
(\mathtt{f}^q, \boldsymbol{v}_h)_{\boldsymbol{X}_h} &= f^q[\boldsymbol{v}_h], \\
(\mathtt{a}^{q,n}, \boldsymbol{v}_h)_{\boldsymbol{X}_h} &= a^q[\boldsymbol{\xi}_n, \boldsymbol{v}_h],
\end{aligned}
$$

for all $\boldsymbol{v}_h \in \boldsymbol{X}_h$ using the Riesz representation theorem. In practice, this corresponds to solving a linear system using the mass matrix associated with the scalar product

$(\cdot,\cdot)_{\boldsymbol{X}_h}$. We finally write

$$\begin{aligned}\|\hat{\boldsymbol{e}}(\boldsymbol{\mu})\|^2_{\boldsymbol{X}_h} = &\sum_{q,m=1}^{Q_{\mathtt{f}}} \overline{\theta^q_{\mathtt{f}}(\boldsymbol{\mu})}\theta^m_{\mathtt{f}}(\boldsymbol{\mu})\,(\mathtt{f}^q,\mathtt{f}^m)_{\boldsymbol{X}_h}\\ &- 2\Re\left[\sum_{n=1}^{N}\sum_{m=1}^{Q_{\mathtt{f}}}\sum_{q=1}^{Q_{\mathtt{a}}} u_n\,\overline{\theta^m_{\mathtt{f}}(\boldsymbol{\mu})}\theta^q_{\mathtt{a}}(\boldsymbol{\mu})\,(\mathtt{f}^m,\mathtt{a}^{q,n})_{\boldsymbol{X}_h}\right]\\ &+ \sum_{n,k=1}^{N}\sum_{q,m=1}^{Q_{\mathtt{a}}} u_n u_k\,\overline{\theta^q_{\mathtt{a}}(\boldsymbol{\mu})}\theta^m_{\mathtt{a}}(\boldsymbol{\mu})\,(\mathtt{a}^{q,n},\mathtt{a}^{m,k})_{\boldsymbol{X}_h}.\end{aligned}$$

Now, one can observe that the quantities

$$\mathtt{R}^1_{q,m} = (\mathtt{f}^q,\mathtt{f}^m)_{\boldsymbol{X}_h},\qquad \mathtt{R}^2_{m,q,n} = (\mathtt{f}^m,\mathtt{a}^{q,n})_{\boldsymbol{X}_h},\qquad \mathtt{R}^3_{q,n,m,k} = (\mathtt{a}^{q,n},\mathtt{a}^{m,k})_{\boldsymbol{X}_h}$$

can be precomputed, i.e., they are parameter independent during the Offline process, once the reduced basis is assembled. Therefore the a posteriori estimate can be computed independently of $\mathcal{N}$ by

$$\begin{aligned}\eta(\boldsymbol{\mu}) = \frac{1}{\beta_{\mathtt{LB}}(\boldsymbol{\mu})}\Bigg(&\sum_{q,m=1}^{Q_{\mathtt{f}}} \overline{\theta^q_{\mathtt{f}}(\boldsymbol{\mu})}\theta^m_{\mathtt{f}}(\boldsymbol{\mu})\,\mathtt{R}^1_{q,m} - 2\Re\left[\sum_{n=1}^{N}\sum_{m=1}^{Q_{\mathtt{f}}}\sum_{q=1}^{Q_{\mathtt{a}}} u_n\,\overline{\theta^m_{\mathtt{f}}(\boldsymbol{\mu})}\theta^q_{\mathtt{a}}(\boldsymbol{\mu})\,\mathtt{R}^2_{m,q,n}\right]\\ &+ \sum_{n,k=1}^{N}\sum_{q,m=1}^{Q_{\mathtt{a}}} u_n u_k\,\overline{\theta^q_{\mathtt{a}}(\boldsymbol{\mu})}\theta^m_{\mathtt{a}}(\boldsymbol{\mu})\,\mathtt{R}^3_{q,n,m,k}\Bigg)^{\frac{1}{2}}.\end{aligned}\tag{3.4}$$

3.3. Implementation of the Successive Constraint Method for complex matrices. The Successive Constraint Method (SCM) is an offline-online procedure where the online part consists of providing, for each new parameter value $\boldsymbol{\mu}\in\boldsymbol{\mathcal{P}}$, a lower bound $\beta_{\mathtt{LB}}$ (and upper bound $\beta_{\mathtt{UB}}$) of the inf-sup constant defined by (3.2), i.e. $0<\beta_{\mathtt{LB}}(\boldsymbol{\mu})\le\beta_h(\boldsymbol{\mu})\le\beta_{\mathtt{UB}}(\boldsymbol{\mu})$. The SCM is discussed in [8, 3, 4] but for the sake of completeness we nevertheless present the method in full detail here. Different from the presentation in [3], where the real and imaginary parts of a complex matrix are decoupled in the SCM, we improve the algorithm by fully utilizing the properties of Hermitian matrices.

The underlying idea of the SCM is that computing the inf-sup constant can be viewed as an optimization problem. We first note that the inf-sup constant introduced in (3.2) can be properly written as

$$\beta_h(\boldsymbol{\mu}) = \inf_{\boldsymbol{v}_h\in\boldsymbol{X}_h}\sup_{\boldsymbol{w}_h\in\boldsymbol{X}_h}\frac{a[\boldsymbol{v}_h,\boldsymbol{w}_h;\boldsymbol{\mu}]}{\|\boldsymbol{v}_h\|_{\boldsymbol{X}_h}\|\boldsymbol{w}_h\|_{\boldsymbol{X}_h}}.$$

Introducing the operator $\mathtt{A}(\boldsymbol{\mu}):\boldsymbol{X}_h\mapsto\boldsymbol{X}_h$ associated to the sesquilinear form $a[\cdot,\cdot;\boldsymbol{\mu}]:\boldsymbol{X}_h\times\boldsymbol{X}_h\mapsto\mathbb{C}$ such that $(\mathtt{A}(\boldsymbol{\mu})\boldsymbol{v}_h,\boldsymbol{w}_h)_{\boldsymbol{X}_h} = a[\boldsymbol{v}_h,\boldsymbol{w}_h;\boldsymbol{\mu}]$ for all $\boldsymbol{v}_h,\boldsymbol{w}_h\in\boldsymbol{X}_h$ we notice that

$$\beta_h(\boldsymbol{\mu}) = \inf_{\boldsymbol{v}_h\in\boldsymbol{X}_h}\frac{\|\mathtt{A}(\boldsymbol{\mu})\boldsymbol{v}_h\|_{\boldsymbol{X}_h}}{\|\boldsymbol{v}_h\|_{\boldsymbol{X}_h}}.$$

Squaring the previous expression results in

$$(\beta_h(\boldsymbol{\mu}))^2 = \inf_{\boldsymbol{v}_h\in\boldsymbol{X}_h}\frac{(\mathtt{A}(\boldsymbol{\mu})\boldsymbol{v}_h,\mathtt{A}(\boldsymbol{\mu})\boldsymbol{v}_h)_{\boldsymbol{X}_h}}{\|\boldsymbol{v}_h\|^2_{\boldsymbol{X}_h}}.$$

We are therefore interested in computing the lowest generalized eigenvalue of the parameter-dependent matrix $\mathtt{A}^*\mathtt{A}(\boldsymbol{\mu})$.

3.3.1. Offline procedure of SCM. Assume for now that the matrix $\mathtt{A}^*\mathtt{A}$ is a linear combination of semi-positive Hermitian matrices, i.e.,

$$\mathtt{A}^*\mathtt{A}(\boldsymbol{\mu}) = \sum_{\hat{q}=1}^{\hat{Q}} z_{\hat{q}}(\boldsymbol{\mu})\mathtt{Z}_{\hat{q}} \tag{3.5}$$

such that all $z_{\hat{q}}$ are real and $\mathtt{Z}_{\hat{q}}$ are semi-positive and Hermitian, and thus have only real non-negative eigenvalues. This is a key-feature of the SCM and a way to achieve this is discussed in Section 3.3.3. We can then continue in a standard fashion as described in [3] by noting that

$$\alpha_h(\boldsymbol{\mu}) = \inf_{\boldsymbol{v}_h \in \boldsymbol{X}_h} \sum_{\hat{q}=1}^{\hat{Q}} z_{\hat{q}}(\boldsymbol{\mu}) \frac{(\boldsymbol{v}_h, \mathtt{Z}_{\hat{q}}\boldsymbol{v}_h)_{\boldsymbol{X}_h}}{\|\boldsymbol{v}_h\|^2_{\boldsymbol{X}_h}}, \tag{3.6}$$

for $\alpha_h(\boldsymbol{\mu}) = (\beta_h(\boldsymbol{\mu}))^2$.

The underlying idea of the SCM is to interpret the right hand side of (3.6) as a minimization problem of the functional

$$\begin{aligned} \mathtt{I} : \boldsymbol{\mathcal{P}} \times \mathbb{R}^{\hat{Q}} &\longrightarrow \mathbb{R} \\ (\boldsymbol{\mu}, \boldsymbol{y}) &\longmapsto \mathtt{I}(\boldsymbol{\mu}, \boldsymbol{y}) = \sum_{\hat{q}=1}^{\hat{Q}} z_{\hat{q}}(\boldsymbol{\mu})\, y_{\hat{q}} \end{aligned}$$

over the set of admissible solutions

$$\boldsymbol{\mathcal{Y}} = \left\{ \boldsymbol{y} = (y_1, \ldots, y_{\hat{Q}}) \in \mathbb{R}^{\hat{Q}} \;\middle|\; \exists\, \boldsymbol{v}_h \in \boldsymbol{X}_h \text{ s.t. } y_{\hat{q}} = \frac{(\boldsymbol{v}_h, \mathtt{Z}_{\hat{q}}\boldsymbol{v}_h)_{\boldsymbol{X}_h}}{\|\boldsymbol{v}_h\|^2_{\boldsymbol{X}_h}}, 1 \le \hat{q} \le \hat{Q} \right\}.$$

Then

$$\alpha_h(\boldsymbol{\mu}) = \min_{\boldsymbol{y} \in \boldsymbol{\mathcal{Y}}} \mathtt{I}(\boldsymbol{\mu}, \boldsymbol{y})$$

and a lower and upper bound can be found by enlarging resp. restricting the admissible set of solution vectors $\boldsymbol{y}$ by introducing $\boldsymbol{\mathcal{Y}}_{\mathtt{UB}} \subset \boldsymbol{\mathcal{Y}} \subset \boldsymbol{\mathcal{Y}}_{\mathtt{LB}}$ and then defining

$$\alpha_{\mathtt{LB}}(\boldsymbol{\mu}) = \min_{\boldsymbol{y} \in \boldsymbol{\mathcal{Y}}_{\mathtt{LB}}} \mathtt{I}(\boldsymbol{\mu}, \boldsymbol{y}), \qquad \text{and} \qquad \alpha_{\mathtt{UB}}(\boldsymbol{\mu}) = \min_{\boldsymbol{y} \in \boldsymbol{\mathcal{Y}}_{\mathtt{UB}}} \mathtt{I}(\boldsymbol{\mu}, \boldsymbol{y}).$$

The remaining question consists of how to design the spaces $\boldsymbol{\mathcal{Y}}_{\mathtt{UB}}$ and $\boldsymbol{\mathcal{Y}}_{\mathtt{LB}}$ in an easy way, but such that any target accuracy can be achieved for the quantity

$$1 - \frac{\alpha_{\mathtt{LB}}(\boldsymbol{\mu})}{\alpha_{\mathtt{UB}}(\boldsymbol{\mu})}.$$

As for the reduced basis method the SCM is an offline-online procedure where during the computing intensive offline stage generalized eigenvalue problems of size $\mathcal{N}$ need to be solved, but where the online stage is $\mathcal{N}$-independent and thus can be used in combination with the online stage of the reduced basis method, as explained in Section 3.2.

Denote by $\boldsymbol{\mathcal{P}_a}$ the restriction of $\boldsymbol{\mathcal{P}}$ to the set of actively varying parameters of the form $a[\cdot,\cdot;\cdot]$. In our case the only active parameter for the sesquilinear form is the wavenumer k. Then, the n-th iteration of the offline procedure takes the following form: Assume that:

1. We know $\alpha_h(\boldsymbol{\mu}_j)$, $1 \le j \le n$, for some parameter values $\mathbb{C}_n = \{\boldsymbol{\mu}_1, \dots, \boldsymbol{\mu}_n\} \subset \boldsymbol{\mathcal{P}_a}$.
2. Let $\Xi \subset \boldsymbol{\mathcal{P}_a}$ be a fine and finite point-set discretization of $\boldsymbol{\mathcal{P}_a}$. For each $\boldsymbol{\mu} \in \Xi$, we know some lower bound $\alpha_{\mathtt{LB}}^{n-1}(\boldsymbol{\mu})$ of $\alpha_h(\boldsymbol{\mu})$ from the previous iteration. For $n = 1$, set $\alpha_{\mathtt{LB}}^{0}(\boldsymbol{\mu}) = 0$.

Thus $\alpha_h(\boldsymbol{\mu}_j)$ corresponds to the smallest eigenvalue of the generalized eigenvalue problem

$$\big(\boldsymbol{v}_h, \mathtt{A}^*\mathtt{A}(\boldsymbol{\mu}_j)\boldsymbol{w}_h^j\big)_{\boldsymbol{X}_h} = \alpha_h(\boldsymbol{\mu}_j)\big(\boldsymbol{v}_h, \boldsymbol{w}_h^j\big)_{\boldsymbol{X}_h}, \qquad \forall \boldsymbol{v}_h \in \boldsymbol{X}_h. \tag{3.7}$$

The collection of smallest eigenvalues provides a set of eigenfunctions $\{\boldsymbol{w}_h^j\}_{j=1}^n$ and corresponding vectors $\{\boldsymbol{y}^j\}_{j=1}^n$ such that

$$(\boldsymbol{y}^j)_{\hat{q}} = \frac{(\boldsymbol{w}_h^j, \mathtt{Z}_{\hat{q}}\boldsymbol{w}_h^j)_{\boldsymbol{X}_h}}{\|\boldsymbol{w}_h^j\|_{\boldsymbol{X}_h}^2}, \qquad 1 \le \hat{q} \le \hat{Q},\ 1 \le j \le n.$$

Then, we set

$$\boldsymbol{\mathcal{Y}}_{\mathtt{UB}}^k(\mathbb{C}_n) = \left\{\boldsymbol{y}^j \,\middle|\, 1 \le j \le n\right\},$$

which is clearly a subset of $\boldsymbol{\mathcal{Y}}$. This means that for $\boldsymbol{\mathcal{Y}}_{\mathtt{UB}}$ we use a finite set of pre-computed vectors $\boldsymbol{y}^j$. Also, computing $\alpha_{\mathtt{UB}}^n(\boldsymbol{\mu}) = \min_{\boldsymbol{y} \in \boldsymbol{\mathcal{Y}}_{\mathtt{UB}}^n} \mathtt{I}(\boldsymbol{\mu}, \boldsymbol{y})$ only consists of forming the functional $\mathtt{I}$ for a finite number of $\boldsymbol{y}^j$, which is independent of $\mathcal{N}$.

On the other hand, for $\boldsymbol{\mathcal{Y}}_{\mathtt{LB}}$ we first define a rectangular box $\boldsymbol{\mathcal{B}} = \prod_{\hat{q}=1}^{\hat{Q}}[\sigma_{\hat{q}}^-, \sigma_{\hat{q}}^+] \subset \mathbb{R}^{\hat{Q}}$ that contains $\boldsymbol{\mathcal{Y}}$ by setting

$$\sigma_{\hat{q}}^- = \inf_{\boldsymbol{v}_h \in \boldsymbol{X}_h} \frac{(\boldsymbol{v}_h, \mathtt{Z}_{\hat{q}}\boldsymbol{v}_h)_{\boldsymbol{X}_h}}{\|\boldsymbol{v}_h\|_{\boldsymbol{X}_h}^2} \qquad \text{and} \qquad \sigma_{\hat{q}}^+ = \sup_{\boldsymbol{v}_h \in \boldsymbol{X}_h} \frac{(\boldsymbol{v}_h, \mathtt{Z}_{\hat{q}}\boldsymbol{v}_h)_{\boldsymbol{X}_h}}{\|\boldsymbol{v}_h\|_{\boldsymbol{X}_h}^2}.$$

This corresponds to the smallest and largest eigenvalues of a generalized eigenvalue problem for each $\hat{q}$ and can be computed once and for all in the beginning of the algorithm. However, in order to have as small as possible a set $\boldsymbol{\mathcal{Y}}_{\mathtt{LB}}$ containing $\boldsymbol{\mathcal{Y}}$ we need to impose some additional restrictions. These constraints will depend on the value of the actual parameter $\boldsymbol{\mu}$ and we distinguish between two types:

1. Constraints based on the exact eigenvalues for some close (in parameter space) parameters out of the set $\mathbb{C}_n$.
2. Constraints based on the previous lower bounds $\alpha_{\mathtt{LB}}^{n-1}$ for some neighbour parameter values.

Observe that, in contrast to $\boldsymbol{\mathcal{Y}}_{\mathtt{UB}}$, the space $\boldsymbol{\mathcal{Y}}_{\mathtt{LB}}$ will change with variation of the parameter $\boldsymbol{\mu}$. We introduce the function that provides close parameter values

$$\mathbb{P}_M(\boldsymbol{\mu}; E) = \begin{cases} M \text{ closest points to } \boldsymbol{\mu} \text{ in } E & \text{if } \operatorname{card}(E) > M, \\ E & \text{if } \operatorname{card}(E) \le M, \end{cases}$$

for $E = \mathbb{C}_n$ and $E = \Xi$. For some M_α and M_p, we then define

$$\begin{aligned} \boldsymbol{\mathcal{Y}}_{\mathtt{LB}}^n(\boldsymbol{\mu}) = \Big\{ \boldsymbol{y} \in \boldsymbol{\mathcal{B}} \,\Big|\, & \mathtt{I}(\boldsymbol{\mu}', \boldsymbol{y}) \ge \alpha_h(\boldsymbol{\mu}'), \quad \forall \boldsymbol{\mu}' \in \mathbb{P}_{M_\alpha}(\boldsymbol{\mu}; \mathbb{C}_n), \\ & \mathtt{I}(\boldsymbol{\mu}', \boldsymbol{y}) \ge \alpha_{\mathtt{LB}}^{n-1}(\boldsymbol{\mu}'), \quad \forall \boldsymbol{\mu}' \in \mathbb{P}_{M_p}(\boldsymbol{\mu}; \Xi) \Big\}. \end{aligned}$$

As consequence, we have the property that

$$\boldsymbol{\mathcal{Y}}^1_{\mathtt{LB}}(\boldsymbol{\mu}) \subset \boldsymbol{\mathcal{Y}}^2_{\mathtt{LB}}(\boldsymbol{\mu}) \subset \ldots \subset \boldsymbol{\mathcal{Y}}^n_{\mathtt{LB}}(\boldsymbol{\mu}) \subset \ldots \subset \boldsymbol{\mathcal{Y}} \subset \ldots \subset \boldsymbol{\mathcal{Y}}^n_{\mathtt{UB}} \subset \ldots \subset \boldsymbol{\mathcal{Y}}^2_{\mathtt{UB}} \subset \boldsymbol{\mathcal{Y}}^1_{\mathtt{UB}}.$$

Note that solving $\alpha^n_{\mathtt{LB}}(\boldsymbol{\mu}) = \min_{\boldsymbol{y} \in \boldsymbol{\mathcal{Y}}^n_{\mathtt{LB}}(\boldsymbol{\mu})} \mathtt{I}(\boldsymbol{\mu}, \boldsymbol{y})$ corresponds to a Linear Program (LP) of $\hat{Q}$ design variables and $2\hat{Q} + M_\alpha + M_p$ conditions. This is independent of $\mathcal{N}$.

Having defined the two sets $\boldsymbol{\mathcal{Y}}^n_{\mathtt{LB}}(\boldsymbol{\mu})$ and $\boldsymbol{\mathcal{Y}}^n_{\mathtt{UB}}$, we can define a greedy selection in order to enrich the space $\mathbb{C}_n$ and build $\mathbb{C}_{n+1}$ at all stages of n. The algorithm is defined as follows.

Given some error tolerance $\mathtt{Tol}$, some initial set $\mathbb{C}_1 = \{\boldsymbol{\mu}_1\}$ and $n = 1$ do:

1. For each $\boldsymbol{\mu} \in \Xi$:
   a. Compute the upper bound $\alpha^n_{\mathtt{UB}}(\boldsymbol{\mu}) = \min_{\boldsymbol{y} \in \boldsymbol{\mathcal{Y}}^n_{\mathtt{UB}}} \mathtt{I}(\boldsymbol{\mu}, \boldsymbol{y})$.
   b. Compute the lower bound $\alpha^n_{\mathtt{LB}}(\boldsymbol{\mu}) = \min_{\boldsymbol{y} \in \boldsymbol{\mathcal{Y}}^n_{\mathtt{LB}}(\boldsymbol{\mu})} \mathtt{I}(\boldsymbol{\mu}, \boldsymbol{y})$.
   c. Define the error estimate $\eta(\boldsymbol{\mu}) = 1 - \frac{\alpha^n_{\mathtt{LB}}(\boldsymbol{\mu})}{\alpha^n_{\mathtt{UB}}(\boldsymbol{\mu})}$.
2. Select $\boldsymbol{\mu}_{n+1} = \arg\max_{\boldsymbol{\mu} \in \boldsymbol{\mathcal{P}}} \eta(\boldsymbol{\mu})$ and set $\mathbb{C}_{n+1} = \mathbb{C}_n \cup \{\boldsymbol{\mu}_{n+1}\}$.
3. If $\max_{\boldsymbol{\mu} \in \boldsymbol{\mathcal{P}}} \eta(\boldsymbol{\mu}) \leq \mathtt{Tol}$, `stop`.
4. Solve the generalized eigenvalue problem (3.7) associated to $\boldsymbol{\mu}_{n+1}$, store $\boldsymbol{y}^{n+1}$.
5. Set $n := n + 1$ and `goto 1`.

3.3.2. Online procedure of SCM. Once the Offline-procedure as described above is finished, we denote $\boldsymbol{\mathcal{Y}}^n_{\mathtt{LB}}(\boldsymbol{\mu})$ by $\boldsymbol{\mathcal{Y}}_{\mathtt{LB}}(\boldsymbol{\mu})$ and $\boldsymbol{\mathcal{Y}}^n_{\mathtt{UB}}$ by $\boldsymbol{\mathcal{Y}}_{\mathtt{UB}}$.

For any arbitrary parameter value $\boldsymbol{\mu} \in \boldsymbol{\mathcal{P}}$, we can then compute a lower bound $\alpha_{\mathtt{LB}}(\boldsymbol{\mu})$ by only retaining the information about $\alpha_h(\boldsymbol{\mu})$ for all $\boldsymbol{\mu} \in \mathbb{C}_n$ and $\alpha_{\mathtt{LB}}(\boldsymbol{\mu})$ for all $\boldsymbol{\mu} \in \Xi$: For any new $\boldsymbol{\mu} \in \boldsymbol{\mathcal{P}}$, find the solution of

$$\alpha_{\mathtt{LB}}(\boldsymbol{\mu}) = \min_{\boldsymbol{y} \in \boldsymbol{\mathcal{Y}}_{\mathtt{LB}}(\boldsymbol{\mu})} \mathtt{I}(\boldsymbol{\mu}, \boldsymbol{y}),$$

which consists again of a Linear Program with $\hat{Q}$ design variables and $2\hat{Q} + M_\alpha + M_p$ constraints.

3.3.3. Affine decomposition for complex matrices. Here we discuss how the affine decomposition (3.5) of the square of the operator can be obtained. Based on the affine decomposition (2.10) we introduce the family of parameter independent operators resp. matrices $\mathtt{A}_q : \boldsymbol{X}_h \mapsto \boldsymbol{X}_h$ such that $(\mathtt{A}_q \boldsymbol{v}_h, \boldsymbol{w}_h)_{\boldsymbol{X}_h} = a^q[\boldsymbol{v}_h, \boldsymbol{w}_h]$, and thus $\mathtt{A}(\boldsymbol{\mu}) = \sum_{q=1}^{Q_\mathtt{a}} \theta^q_\mathtt{a}(\boldsymbol{\mu})\, \mathtt{A}_q$. As a consequence,

$$\begin{aligned}
\mathtt{A}^*\mathtt{A}(\boldsymbol{\mu}) &= \sum_{q,m=1}^{Q_\mathtt{a}} \overline{\theta^m_\mathtt{a}(\boldsymbol{\mu})} \theta^q_\mathtt{a}(\boldsymbol{\mu})\, \mathtt{A}^*_m \mathtt{A}_q \\
&= \sum_{q=1}^{Q_\mathtt{a}} \overline{\theta^q_\mathtt{a}(\boldsymbol{\mu})} \theta^q_\mathtt{a}(\boldsymbol{\mu})\, \mathtt{A}^*_q \mathtt{A}_q + \sum_{q=1}^{Q_\mathtt{a}} \sum_{m=q+1}^{Q_\mathtt{a}} \left[\overline{\theta^m_\mathtt{a}(\boldsymbol{\mu})} \theta^q_\mathtt{a}(\boldsymbol{\mu})\, \mathtt{A}^*_m \mathtt{A}_q + \overline{\theta^q_\mathtt{a}(\boldsymbol{\mu})} \theta^m_\mathtt{a}(\boldsymbol{\mu})\, \mathtt{A}^*_q \mathtt{A}_m \right].
\end{aligned}$$

For sake of short notation denote $z_{mq} = \overline{\theta_{\mathtt{a}}^m(\boldsymbol{\mu})}\theta_{\mathtt{a}}^q(\boldsymbol{\mu})$ and observe that $z_{qm} = \overline{z_{mq}}$. Therefore

$$\begin{aligned}
&z_{mq}\mathtt{A}_m^*\mathtt{A}_q + z_{qm}\mathtt{A}_q^*\mathtt{A}_m \\
&\qquad = z_{mq}\mathtt{A}_m^*\mathtt{A}_q + \overline{z_{mq}}\mathtt{A}_q^*\mathtt{A}_m \\
&\qquad = \Re(z_{mq})(\mathtt{A}_m^*\mathtt{A}_q + \mathtt{A}_q^*\mathtt{A}_m) + i\Im(z_{mq})(\mathtt{A}_m^*\mathtt{A}_q - \mathtt{A}_q^*\mathtt{A}_m) \\
&\qquad = \Re(z_{mq})(\mathtt{A}_m + \mathtt{A}_q)^*(\mathtt{A}_m + \mathtt{A}_q) + \Im(z_{mq})(\mathtt{A}_m + i\mathtt{A}_q)^*(\mathtt{A}_m + i\mathtt{A}_q) \\
&\qquad\quad - [\Re(z_{mq}) + \Im(z_{mq})]\,\mathtt{A}_q^*\mathtt{A}_q - [\Re(z_{mq}) + \Im(z_{mq})]\,\mathtt{A}_m^*\mathtt{A}_m,
\end{aligned}$$

respectively

$$\begin{aligned}
&\mathtt{A}^*\mathtt{A}(\boldsymbol{\mu}) \\
&= \sum_{q=1}^{Q_{\mathtt{a}}} \left[z_{qq} - \sum_{m=q+1}^{Q_{\mathtt{a}}} [\Re(z_{mq}) + \Im(z_{mq})] \right] \mathtt{A}_q^*\mathtt{A}_q - \sum_{q=1}^{Q_{\mathtt{a}}} \sum_{m=q+1}^{Q_{\mathtt{a}}} [\Re(z_{mq}) + \Im(z_{mq})]\,\mathtt{A}_m^*\mathtt{A}_m \\
&\quad + \sum_{q=1}^{Q_{\mathtt{a}}} \sum_{m=q+1}^{Q_{\mathtt{a}}} \Re(z_{mq})(\mathtt{A}_m + \mathtt{A}_q)^*(\mathtt{A}_m + \mathtt{A}_q) + \Im(z_{mq})(\mathtt{A}_m + i\mathtt{A}_q)^*(\mathtt{A}_m + i\mathtt{A}_q) \\
&= \sum_{q=1}^{Q_{\mathtt{a}}} \left[z_{qq} - \sum_{m=1}^{q-1} [\Re(z_{qm}) - \Im(z_{qm})] - \sum_{m=q+1}^{Q_{\mathtt{a}}} [\Re(z_{mq}) + \Im(z_{mq})] \right] \mathtt{A}_q^*\mathtt{A}_q \\
&\quad + \sum_{q=1}^{Q_{\mathtt{a}}} \sum_{m=q+1}^{Q_{\mathtt{a}}} \Re(z_{mq})(\mathtt{A}_m + \mathtt{A}_q)^*(\mathtt{A}_m + \mathtt{A}_q) + \Im(z_{mq})(\mathtt{A}_m + i\mathtt{A}_q)^*(\mathtt{A}_m + i\mathtt{A}_q),
\end{aligned}$$

where the second equality follows from reordering the coefficients corresponding to the terms $\mathtt{A}_m^*\mathtt{A}_m$ and interchanging the indices m and q. We are therefore able to write $\mathtt{A}^*\mathtt{A}$ as a linear combination of semi-positive Hermitian matrices, i.e.,

$$\mathtt{A}^*\mathtt{A}(\boldsymbol{\mu}) = \sum_{\hat{q}=1}^{\hat{Q}} z_{\hat{q}}(\boldsymbol{\mu})\mathtt{Z}_{\hat{q}}$$

for $\hat{Q} = Q_{\mathtt{a}}^2$ and using an appropriate re-indexing.

4. Numerical results. In the following we provide a number of tests to verify the results above and demonstrate the accuracy and efficiency of the overall framework. To keep things simple and consistent, we consider scattering examples based on the shapes illustrated in Figures 4.1, 4.2, and 4.3 through their meshes.

4.1. Successive Constraint Method. We first test the SCM on its own, unrelated to the reduced basis method.

4.1.1. Influence of M_α and M_p. The first series of tests consists of analyzing the dependence of the convergence on M_α and M_p. Higher values of those two numbers implies more work for evaluating the lower bound of the inf-sup constant, playing an important role during the online stage of the reduced basis method. The convergence of the SCM is however expected to be faster than for smaller values.

To analyze the dependence on the convergence of the SCM we consider the sphere discretized as illustrated in Figure 4.1 and a range of wave-numbers $k \in [1, 3]$. The profile of the inf-sup constant is presented in Figure 4.4. Note the presence of the

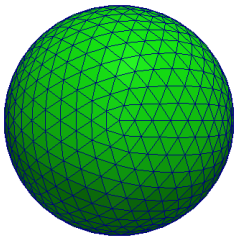

FIG. 4.1. *Coarse sphere.*

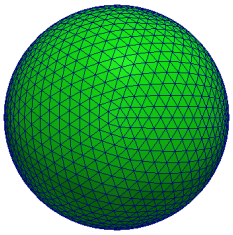

FIG. 4.2. *Fine sphere.*

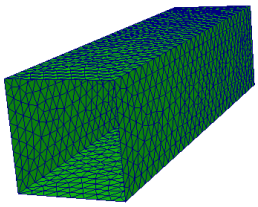

FIG. 4.3. *Cavity.*

first interior resonant wave number at $k_1 = 2.743$. Figure 4.5 shows the convergence for varying $M = M_p = M_\alpha = 5, 10, 15, 20, 25$, Figures 4.6 and 4.7 the convergence for fixed $M_p = 15$ resp. $M_\alpha = 15$ and $M_\alpha = 5, 10, 15, 20, 25$ resp. $M_p = 5, 10, 15, 20, 25$. We notice that for this example it is required that $M_\alpha > 10$ for a proper convergence and it seems that M_p does not have a major influence, at least in this particular example, on the convergence rate.

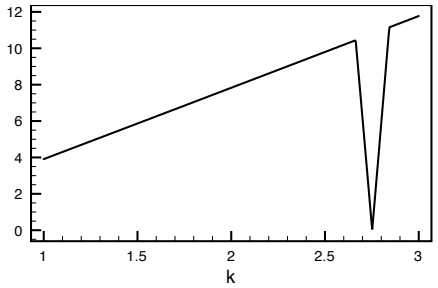

FIG. 4.4. *Profile of the inf-sup constant for* $k \in [1, 3]$.

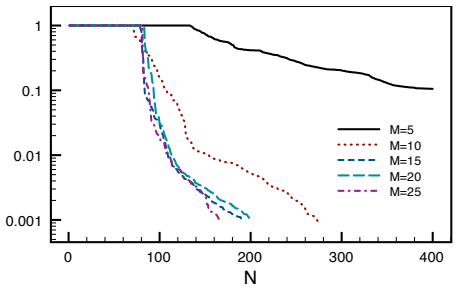

FIG. 4.5. *Convergence behavior of the SCM under variation of* $M = M_\alpha = M_p = 5, 10, 15, 20, 25$.

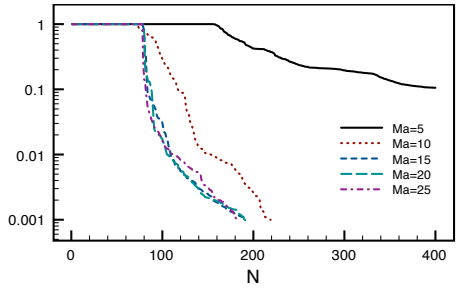

FIG. 4.6. *Convergence behavior of the SCM under variation of* $M_\alpha = 5, 10, 15, 20, 25$ *for a fixed* $M_p = 15$.

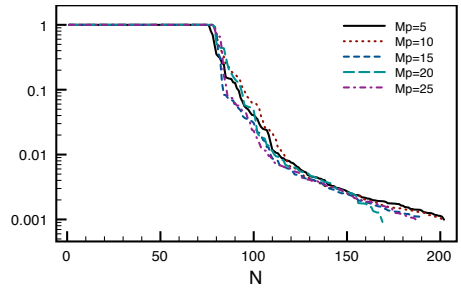

FIG. 4.7. *Convergence behavior of the SCM under variation of* $M_p = 5, 10, 15, 20, 25$ *for a fixed* $M_\alpha = 15$.

Physically more interesting is to increase the interval of wave numbers under consideration. We now consider $k \in [1, 5]$ which requires the use of a finer discretization of the sphere, c.f. Figure 4.2, to guarantee 10 degrees of freedom per wavelength.

The parameters of the SCM are set to `Tol` $= 0.1$, $M_\alpha = M_+ = 20$ and Figure 4.8 shows the convergence of the SCM in this case. Figure 4.9 plots the lower and

upper bound of the inf-sup constant and the parameter values that were chosen during the greedy algorithm. One can observe that the resonant wave-numbers $k_1 = 2.743$, $k_2 = 3.870$, $k_3 = 4.493$ and $k_4 = 4.973$ (c.f. [1, Table 6.1])are causing the inf-sup constant to be (close to) zero.

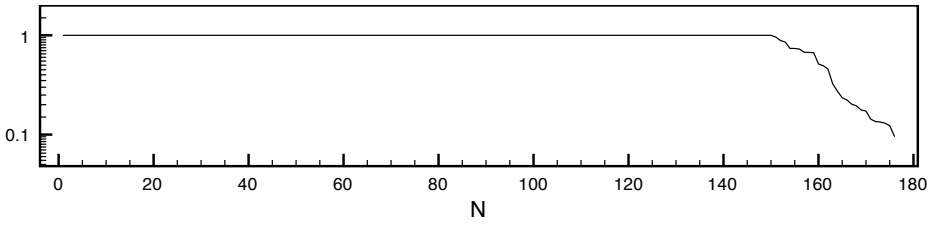

FIG. 4.8. *Convergence of SCM for $k \in [1,5]$ using a sphere as geometry (Figure 4.2) and* `Tol` $= 0.1$, $M_\alpha = M_+ = 20$.

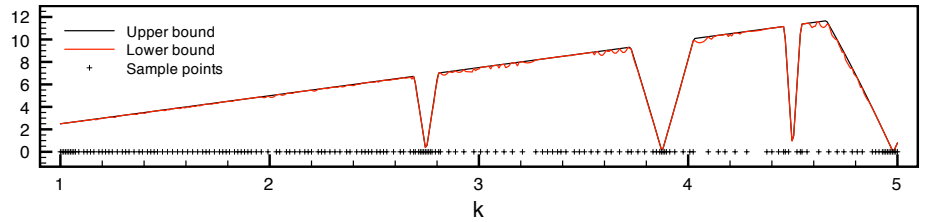

FIG. 4.9. *Lower and upper bound of the inf-sup constant for $k \in [1,5]$ using a sphere as geometry (Figure 4.2) and* `Tol` $= 0.1$, $M_\alpha = M_+ = 20$. *In addition, the chosen parameter values by the SCM are indicated.*

We finally consider the cavity illustrated in Figure 4.3 for a range of wave-numbers $k \in [10, 20]$, `Tol` $= 10^{-3}$ and $M_\alpha = M_+ = 20$. The corresponding lower and upper bound (indistinguishable) of the inf-sup constant is illustrated in Figure 4.11. One can observe the various "negative peaks" where the inf-sup constant drops locally due to near-resonances. We notice that the constant varies two orders of magnitude which may have an essential impact on the a posteriori estimates of the reduced basis method.

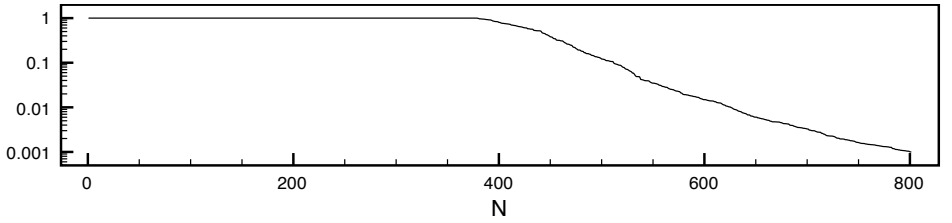

FIG. 4.10. *Convergence of SCM for $k \in [1,5]$ using the cavity (Figure 4.3) as geometry and* `Tol` $= 10^{-3}$, $M_\alpha = M_+ = 20$.

4.2. Certified Reduced Basis Method. In this section, we present numerical results of the certified reduced basis method, which relies on the SCM in order to provide accurate a posteriori estimates.

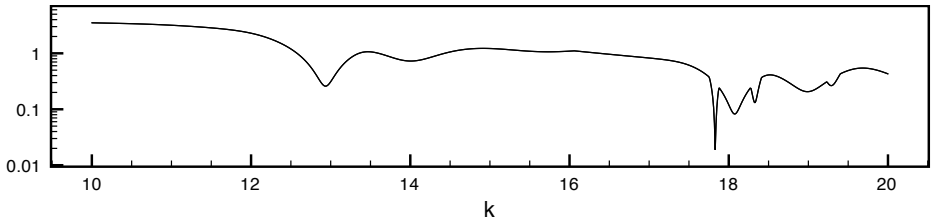

FIG. 4.11. *Lower and upper bound (indistinguishable) of the inf-sup constant for* $k \in [10, 20]$ *using the cavity (Figure 4.3) as geometry and* $\texttt{Tol} = 10^{-3}$, $M_\alpha = M_+ = 20$.

We first consider the problem associated with the sphere presented in Figure 4.2 and an interval of wave-numbers $k \in [4.52, 4.95]$. As indicated in Figure 4.9 the EFIE is not well-posed at the resonant wave-numbers and need to be excluded. Figure 4.12 shows the convergence of the maximal error (over the parameter space and measured in the $H(\mathrm{div}, \Omega)$-norm) and the residual-based error estimation η_N, which, as described in Proposition 3.1, is an upper bound of the error. The error profile during the last iteration ($N = 4$) of the greedy-algorithm of the reduced basis method is illustrated in Figure 4.13 as well as the chosen parameter values.

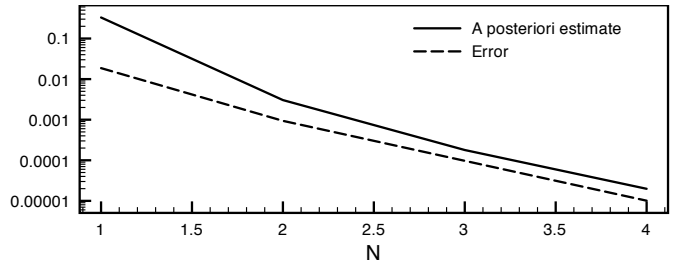

FIG. 4.12. *Maximal error and a posteriori error estimation over the parameter space at each step of the greedy-algorithm during the Reduced Basis assembling process for a sphere as in Figure 4.2 with* $k \in [4.52, 4.95]$.

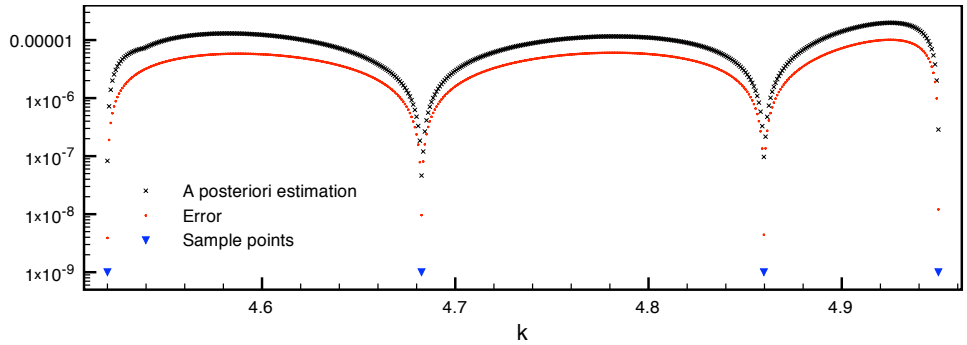

FIG. 4.13. *Error profile over the parameter space at the last iteration of the greedy-algorithm during the Reduced Basis assembling process for a sphere as in Figure 4.2 with* $k \in [4.52, 4.95]$.

Further, we reconsider the example using the cavity (Figure 4.3) as geometry and having parameters $k \in [10, 20]$ for

$$\hat{\boldsymbol{d}} = -(\sin(\pi/2), 0, \cos(\pi/2)) \qquad \text{and} \qquad \hat{\boldsymbol{d}}_0 = (\sin(\pi/2), 0, \cos(\pi/2)),$$

so that we are considering the backscattering (monostatic) RCS. The polarization is set to $\hat{\boldsymbol{p}} = \frac{1}{\sqrt{2}}(1, 0, -1)$. Observe that the only active parameter here is the wave-number k. In Figure 4.14 we plot the convergence of the residual a posteriori estimate and the corresponding error measured in the $\boldsymbol{H}(\mathrm{div})$-norm. Figure 4.15 illustrates the error profile over the parameter space at the last iteration ($N = 23$) and for $N = 16$ whereas Figure 4.16 shows the efficiency index

$$\mathrm{eff}(\boldsymbol{\mu}) = \frac{\eta(\boldsymbol{\mu})}{\|\boldsymbol{u}_h(\boldsymbol{\mu}) - \boldsymbol{u}_N(\boldsymbol{\mu})\|_{\boldsymbol{X}_h}}$$

depending on $\boldsymbol{\mu} \in \boldsymbol{\mathcal{P}}$ for three different values of N. We observe that the a posteriori estimate η_N is indeed an upper bound of the error (in the $H(\mathrm{div}, \Omega)$-norm) as indicated by Proposition 3.1 except close to parameter values that are chosen during the sampling strategy. At such points, the error and error estimate are very small (even theoretically equal to zero at the sample points), in practical computations rounding errors however dominate. This may lead that the efficiency index is smaller than one.

Figure 4.17 illustrates the RCS signal for values $k \in [10, 20]$ based on the reduced basis approximation and the truth solver (the boundary element method), including the upper and lower error bars according to Proposition 3.5 for $N = 21$, $N = 22$ and at the final iteration $N = 23$.

Finally, in Figure 4.18 the error in the RCS (compared to the RCS computed the truth solver which is the boundary element method in our case) and the certified error bound is shown. We observe that the error estimates well certify the error and that the estimation is in general pessimistic.

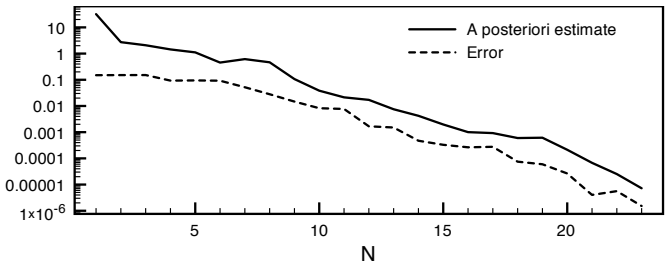

FIG. 4.14. *Maximal error and a posteriori error estimation over the parameter space at each step of the greedy-algorithm during the Reduced Basis assembling process for a cavity as in Figure 4.3 with* $k \in [10, 20]$.

5. Concluding remarks. In the present work we have developed a complete framework for the certified reduced basis method applied to the parametrized electric field integral equation (EFIE). The parameters consist of the wave-number, the angle and polarization of the incident plane wave.

We presented in detail how the rigorous *a posteriori* estimates, which are key ingredients to certify the error tolerance of the model reduction, are developed in the present case. An important feature is to give an estimate of the inf-sup constant, that is parameter dependent, by means of the successive constraint method (SCM). One particularity of the EFIE is that the SCM needed to be generalized to complex matrices. Further, we derived error estimates that certify the error of the radar cross section, which is a non-linear functional of the unknowns of the EFIE. Finally, we presented some numerical examples to test the performance of the SCM and the reduced basis method.

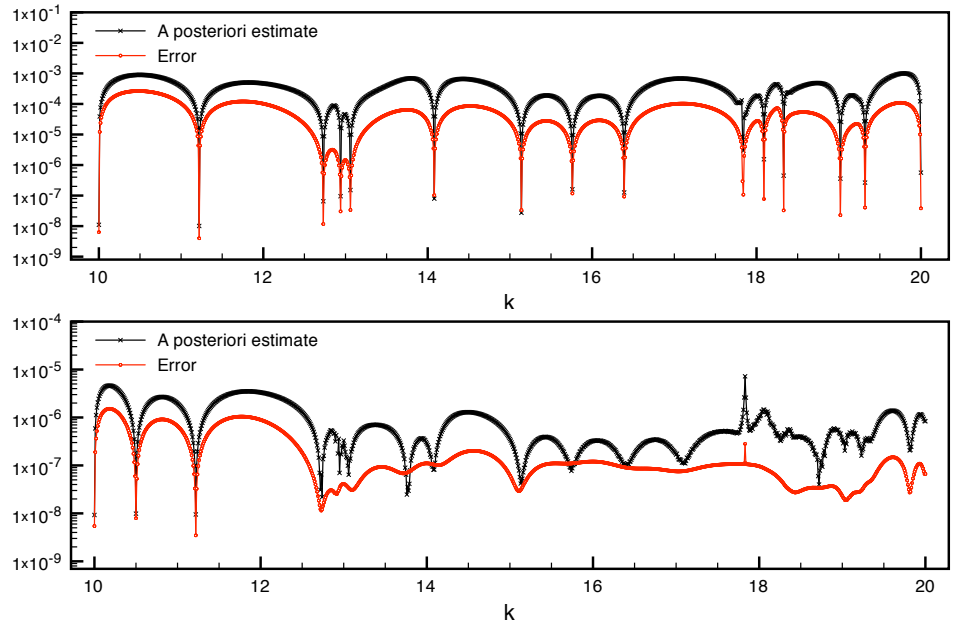

FIG. 4.15. *Error profile over the parameter space at iteration $N = 16$ (top) and $N = 23$ (bottom) of the greedy-algorithm during the Reduced Basis assembling process for a cavity as in Figure 4.3 with $k \in [10, 20]$.*

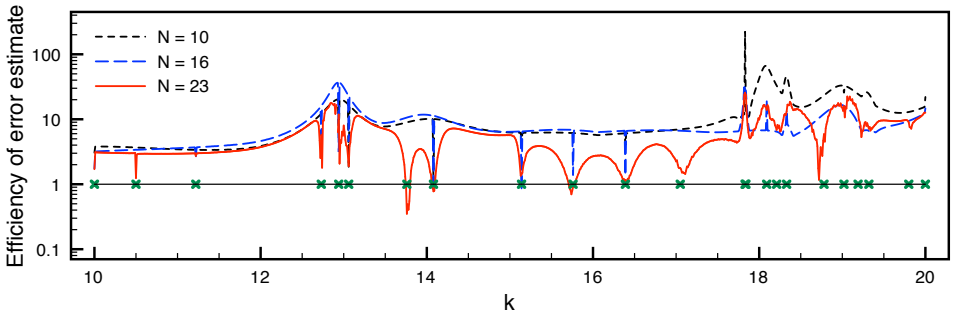

FIG. 4.16. *Efficiency of the error estimator over the parameter space for $N = 10, 16, 23$ during the greedy-algorithm for the Reduced Basis assembling process for a cavity as in Figure 4.3 with $k \in [10, 20]$ and the sampling points for $N = 23$.*

Acknowledgement. The first and third authors acknowledge partial support by OSD/AFOSR FA9550-09-1-0613.

REFERENCES

[1] J. H. Bramble, T. V. Kolev, and J. E. Pasciak, *The approximation of the Maxwell eigenvalue problem using a least-squares method*, Math. Comp., 74, (2005) pp 1575–1598.

[2] A. Buffa, S.H. Christiansen, *The electric field integral equation on Lipschitz screens: definitions and numerical approximation*, Numer. Math. 94 (2) (2003) 229–267.

[3] Y. Chen, J. S. Hesthaven, Y. Maday, and J. Rodriguez, *Improved successive constraint method based a posteriori error estimate for reduced basis approximation of 2d Maxwells problem*, ESAIM: M2AN, 43 (2009), pp. 1099–1116.

[4] Y. Chen, J. S. Hesthaven, Y. Maday, and J. Rodriguez, *Certified reduced basis methods and output bounds for the harmonic maxwell equations*, SIAM J. Sci. Comput., 32(2010),

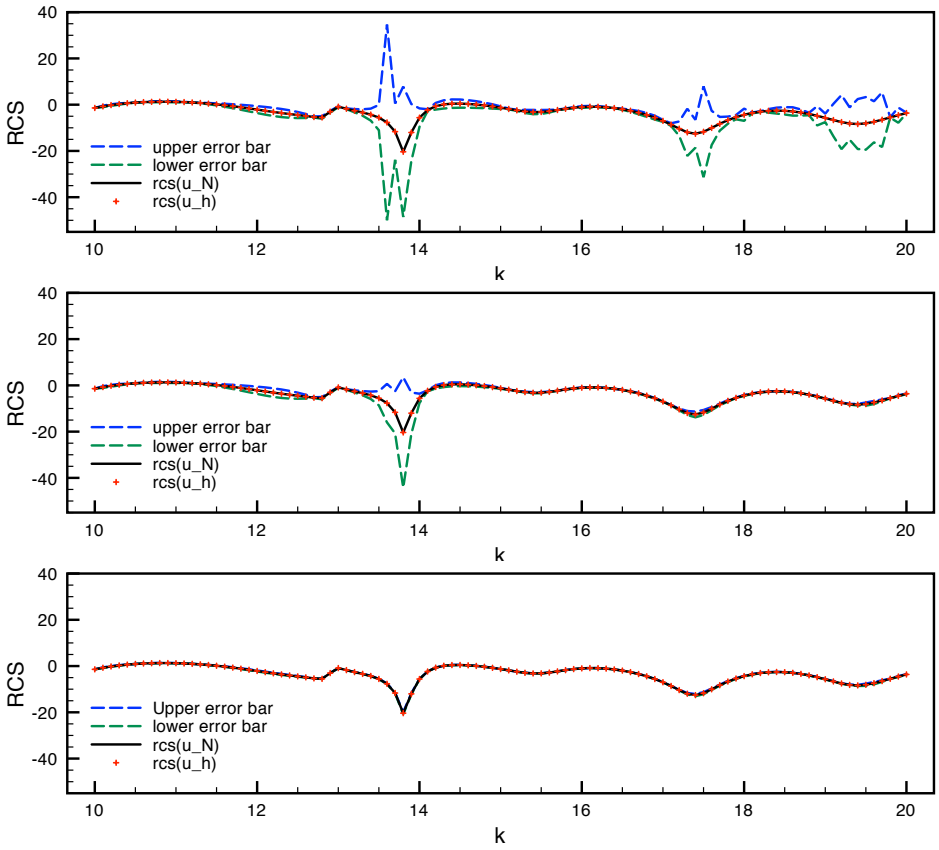

FIG. 4.17. *The radar cross section (RCS) for* $k \in [10, 20]$ *using the reduced basis approximation and the boundary element method including error bars for* $N = 21$ *(top),* $N = 22$ *(middle) and* $N = 23$ *(bottom).*

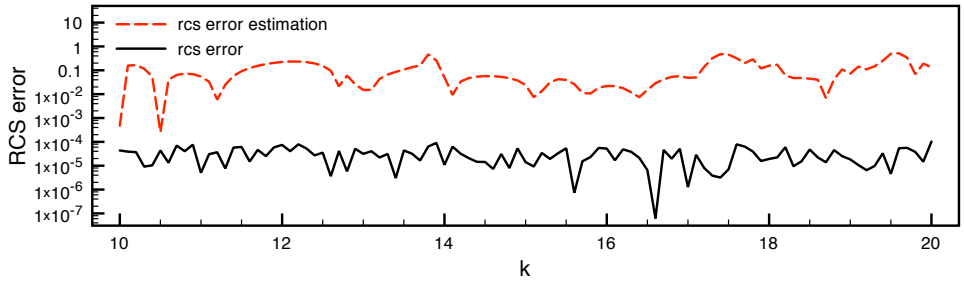

FIG. 4.18. *The error of the radar cross section (RCS) for* $k \in [10, 20]$ *using the reduced basis approximation and the certified error estimation for the RCS at the final iteration* $N = 23$.

pp. 970-996.

[5] B. FARES, J.S. HESTHAVEN, Y. MADAY, AND B. STAMM, *The reduced basis method for the electric field integral equation*, J. Comput. Phys. 230(14), 2011, pp.5532–5555.

[6] R. HARRINGTON, *Field Computation by Moment Methods*, Macmillan Company, New York, 1968.

[7] R. HIPTMAIR, C. SCHWAB, *Natural boundary element methods for the electric field integral equation on polyhedra*, SIAM J. Numer. Anal. 40 (1) (2002) 66–86.

[8] D. B. P. HUYNH, G. ROZZA, S. SEN, AND A. T. PATERA, *A successive constraint linear opti-*

mization method for lower bounds of parametric coercivity and inf-sup stability constants, C. R. Acad. Sci. Paris, Ser. I, 345 (2007), pp. 473–478.

[9] D.B.P. Huynh, D.J. Knezevic, Y. Chen, J.S. Hesthaven, A.T. Patera, *A Natural-Norm Successive Constraint Method for Inf-Sup Lower Bounds*, CMAME, 199 (2010) 1963–1975

[10] P. Oswald, *Multilevel norms for $H^{-1/2}$*, Computing 61 (1998), 235–255.

[11] A.T. Patera and G. Rozza, *Reduced Basis Approximation and A Posteriori Error Estimation for Parametrized Partial Differential Equations*, Version 1.0, Copyright MIT 2006, to appear in (tentative rubric) MIT Pappalardo Graduate Monographs in Mechanical Engineering.

[12] P.-A. Raviart, J.M. Thomas, *A mixed finite element method for 2nd order elliptic problems*, Lecture Notes in Math., vol. 606, 1977, pp. 292–315.

[13] G. Rozza, D.B.P. Huynh, and A.T. Patera, *Reduced basis approximation and a posteriori error estimation for affinely parametrized elliptic coercive partial differential equations - Application to transport and continuum mechanics*, Archives of Computational Methods in Engineering 15(3):229 - 275, 2008.